NJC

Accepted Manuscript

This is an *Accepted Manuscript*, which has been through the Royal Society of Chemistry peer review process and has been accepted for publication.

Accepted Manuscripts are published online shortly after acceptance, before technical editing, formatting and proof reading. Using this free service, authors can make their results available to the community, in citable form, before we publish the edited article. We will replace this *Accepted Manuscript* with the edited and formatted *Advance Article* as soon as it is available.

You can find more information about *Accepted Manuscripts* in the Information for Authors.

Please note that technical editing may introduce minor changes to the text and/or graphics, which may alter content. The journal's standard Terms & Conditions and the Ethical guidelines still apply. In no event shall the Royal Society of Chemistry be held responsible for any errors or omissions in this *Accepted Manuscript* or any consequences arising from the use of any information it contains.

ROYAL SOCIETY OF CHEMISTRY

www.rsc.org/njc

Synthesis, X-ray crystal structure, DNA/protein binding and DNA Cleavage Studies of Novel Copper(II) Complexes of N-substituted isatin thiosemicarbazone ligands

Mathiyan Muralisankar, [a] **Nattamai S. P. Bhuvanesh**[b] **and Anandaram Sreekanth**[a*]

Abstract

A new series of N-substituted isatin thiosemicarbazone ligands (**L1–L5**) and their copper(II) complexes [Cu(II)(ITSC)] were synthesized and characterized by elemental analyses and UV Visible, FT-IR, ^{1}H & ^{13}C NMR / EPR and mass spectroscopic techniques. The molecular structures of **L1-L5**, and **3** were confirmed by single crystal X-ray crystallography. The X-ray diffraction studies of the complexes reveal the square planar geometry. The interaction of calf thymus (CT) DNA and bovine serum albumin (BSA) with the copper(II) complexes was explored using absorption and emission spectral methods. Spectral evidences show intercalative mode of DNA binding with the copper(II) complexes. The DNA cleavage study shows that the complexes cleaved DNA without any external agents. Spectral evidences also support the binding property of the complexes with the protein. The alterations in the secondary structure of the protein by the copper(II) complexes (1–5) were confirmed by synchronous and three dimensional fluorescence spectroscopic studies.

---

[a] Department of Chemistry, National Institute of Technology, Tiruchirappalli - 620 015, India.

*****Corresponding Author: E-mail address: sreekanth@nitt.edu; Tel: +91 431 2503642

[b] Department of Chemistry, Texas A & M University, College Station, TX 77842, USA

Electronic supplementary information (ESI) available: Crystallographic data for the structures reported in this paper have been deposited with the Cambridge Crystallographic Data Centre (CCDC) as supplementary publication numbers (CCDC 1418905, CCDC 1418936, CCDC 1418933, CCDC 1418935, CCDC 1418934 and CCDC 1418937 for L1, L2, L3, L4, L5, and **3** respectively). Copies of the data can be obtained free of charge from the CCDC (12 Union Road, Cambridge CB2 1EZ, UK; Tel.: + 44-1223-336408; Fax: + 44-1223-336003; e-mail: deposit@ccdc.cam.ac.uk ; Web site http://www.ccdc.cam.ac.uk).

1. Introduction

Cancer remains the major cause of death in the world even though there is an effective development in the novel anticancer drugs. The reason for this scenario is due to the drug resistance or undesirable side effects of anticancer drugs. Metallo anticancer drug discovery remains as one of the progressive areas of pharmaceutical research. Metal complexes which binds and cleaves DNA under physiological conditions are considered as potential candidates which can be used as therapeutic agents in medicinal applications and for genomic research.[1-6] Although many transition metal complexes were reported as anticancer agents and some of them were under clinical trials, developing copper containing metallodrug gains special significance because of its biocompatibility. Copper complexes have emerged as the best candidates towards the search of the metal complexes of biological importance.[7-9] Synthetic copper(II) complexes have been reported as potential anticancer and cancer inhibiting agents [10,11] and number of copper complexes [12,13] have been found to be active both *in vitro* and *in vivo*. Similarly, protein was also serves as one of the main molecular targets in the action of anticancer agents since it is involved in the important mechanisms in the cell.[14] The interaction between protein and drugs provides valuable information on the structural features that determine the therapeutic effectiveness of drugs and also to study the pharmacological response of drugs.[15,16] Therefore the interaction studies of protein with metal complexes gained paramount importance.

Thiosemicarbazones and their derivatives are versatile ligands as they exhibit various binding modes with transition and some main group metals. Thiosemicarbazones generally bind to a metal ion, either in the thione form (1) or in the thiol form (2), as bidentate N, S donor ligands forming five membered chelate rings. However, incorporation of a third donor site (D) into these thiosemicarbazone ligands, linked to the carbonylic carbon via one or two intervening atoms, normally results in D, N, S tricoordination (3) (Fig. 1).[17-19] The fascinating interest in thiosemicarbazone chemistry is also due their biological activities[20] and medicinal properties against bacterial and viral infections, tuberculosis, leprosy, coccidiosis and malaria.[21-25] The biological activity will still be enhanced on complexation with transition metals.[26-29] Copper complexes containing thiosemicarbazones are also found to have various biological applications. Coordination of such thiosemicarbazone ligands with metal ions has been found to produce synergistic effects on the antiproliferative activities of the parent ligands.[30]

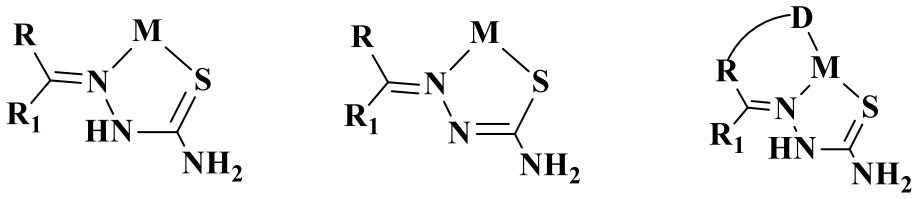

1 **2** **3**

Fig. 1 Different coordination modes of thiosemicarbazone.

The chemistry of copper complexes containing thiosemicarbazones are of great interest because of its different coordination behavior and biological applications.[31,32] Cu(II) complexes containing heterocyclic thiosemicarbazone ligands are found to have various biological applications. In this aspect, a great deal of attention has been focused on the complexes formed by copper metal ions with thiosemicarbazones. These stimulated us to develop heterocyclic thiosemicarbazones based Cu(II) complexes for biological applications. Herein we report the synthesis and characterization of Cu(II) complexes containing heterocyclic thiosemicarbazone ligands. The interaction of the Cu(II) complexes with CT-DNA and BSA was studied using spectroscopic methods. We have also carried out the DNA cleavage experiments by the Cu(II) complexes.

2. Results and discussion

2.1. Synthesis

The substituted heterocyclic based ligands (**L1–L5**) were synthesized by a condensation reaction from substituted heterocyclic based ketone and pyrrolidine thiosemicarbazide (Scheme **1**). The Cu(II) complexes were synthesized using $CuCl_2 \cdot 2H_2O$ as the precursor (Scheme **2**). All the ligands and their Cu(II) complexes were characterized by elemental analyses and/or various spectroscopic techniques. The molecular structure of **L1-L5** and **3** were confirmed by single crystal X-ray diffraction studies.

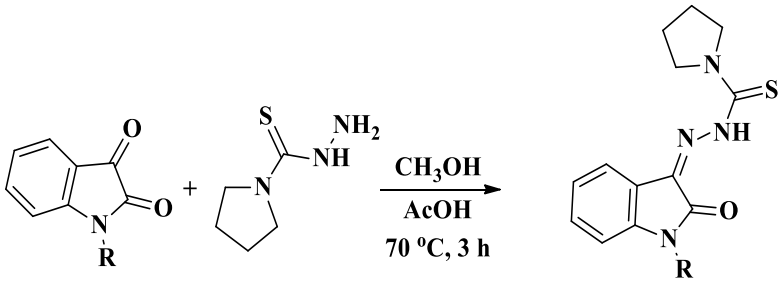

R = H (L1), C_3H_3 (L2), C_3H_5 (L3), C_5H_{11}(L4) or C_7H_7 (L5)

Scheme 1 Synthesis of heterocyclic based thiosemicarbazone.

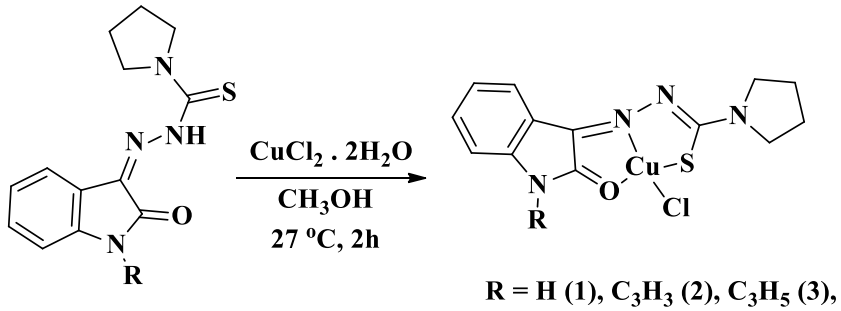

Scheme 2 Synthesis of copper(II) complexes.

2.2. Spectroscopy

The tentative assignments of the significant electronic spectral bands of ligands showed two bands around 278-281 and 349-351 nm, which correspond to $\pi \rightarrow \pi^*$ and $n \rightarrow \pi^*$ transitions respectively. UV-visible spectra of complexes, taken in DMF at same concentration i.e. for fresh solution day one and after five days. There was no distinct changes observed in the UV-visible bands which clearly shows that the copper(II) complexes are stable in test solution. The spectra of the complexes exhibited three bands. Two bands appeared around 269-273 and 373-382 nm, which correspond to intraligand and ligand to metal charge transfer (LMCT) transitions respectively. A band in the region 417-429 nm corresponds to $d \rightarrow d$ transition. Appearance of this band is a combination of all the three spin allowed transitions viz., $^2B_{1g} \rightarrow {}^2A_{1g}$ ($d_{x^2-y^2} \rightarrow d_{z^2}$), $^2B_{1g} \rightarrow {}^2B_{2g}$ ($d_{x^2-y^2} \rightarrow d_{xy}$), $^2B_{1g} \rightarrow {}^2E_g$ ($d_{x^2-y^2} \rightarrow d_{xy}, d_{yz}$), which are almost degenerate and are difficult hence to resolve.

In the FT-IR spectra of the ligands, two bands were observed for N-H groups in the range of 3412-3167 cm^{-1}. The C=N stretching frequency of the ligands was observed at 1582-1540 cm^{-1}. The C=O and C=S stretching frequencies appeared around 1688-1676 cm^{-1} and 1284-1251 cm^{-1} respectively. During on complexation there is a decrease in carbonyl, thiocarbonyl and azomethine stretching frequencies, which suggested that thiosemicarbazones coordinate to copper(II) through sulfur, carbonyl oxygen and the azomethine nitrogen atoms. The Cu-N stretching frequencies for azomethine nitrogen are observed around 388-399 cm^{-1}. The presence of a new bands in the 326-349 cm^{-1} range which is assignable to Cu-S is another indication of

involvement of sulfur coordination. Bands at 308-319 cm^{-1} for the complexes are due to Cu-Cl stretching suggestive for terminally bonded chlorine.[33]

The ^{1}H NMR spectra of the ligands (**L1-L5**), H–N–C=S protons resonate at around 13.33-13.51 ppm. The signals of pyrrolidine protons in the all ligands appeared around 4.01-1.97 ppm. The single around 7.80-6.77 ppm corresponding to aromatic protons of the ligands (**L1-L5**). The signal of amide N–H (**L1**) proton appeared at 11.06 ppm. In the ligand **L2** and **L3** the CH_2, propargyl CH and allyl CH protons shows signal around 4.57, 4.40 and 5.91-5.81 ppm respectively. The signal at 4.96 ppm corresponding to benzyl CH_2 protons of the ligand **L5**. ^{13}C NMR spectra of the ligands showed resonances due to thiocarbonyl (C=S), carbonyl carbon (C=O) and imine carbon (C=N) in the regions 176.3-176.4, 160.8-162.7 and 139.7-141.9 ppm respectively. In the ligand **L3**, allyl carbon singles appeared at 118.1, 53.2 and 48.9 ppm. The signal regions 53.0 ppm corresponding to benzyl carbon of **L5**. The pyrrolidine carbons appeared at 30.9-29.7, 28.9, 26.4 and 24.2 ppm respectively. Chemical shift of all other aromatic and aliphatic protons/carbons was observed in the expected region.[34]

All the compounds are EPR active due to the presence of an unpaired electron. The oxidation state of the central copper atom in the complexes was confirmed by the measurements of EPR spectroscopy. X-band CW EPR spectra of the Cu(II) complexes were recorded at LNT. The observation of quartet hyperfine structure on the parallel component is due to the interaction of unpaired electron of Cu(II) with Cu having nuclear spin I = 3/2. [35,36] All the complexes showed well resolved quartet hyperfine splitting typical of square planar Cu(II) system (Fig. 2), which was confirmed by single crystal XRD technique. For all the complexes $g_{\|} > g\perp$ suggesting that the system is axial. The trend in the g value ($g_{\|} > g\perp > 2.00$) and the value of exchange interaction term ($G > 4.0$) suggested that the unpaired electron of Cu(II) ion is present in the $dx^2–y^2$ orbital (Table 1).

2.3. Single crystal X-ray crystallographic studies

Thermal ellipsoid plots of ligands (**L1-L5**) and complexes (**3**) with the atomic labelling schemes are shown in the Figs. 3-8. Crystal data and selected inter atomic bond lengths and angles are given in the Tables 2-5. The five- and six-membered rings of the isatin in **L1, L2, L3, L4** and **L5** are virtually planar. The crystal structures of the ligands showed the existence of an intra-molecular hydrogen bond between N–H and carbonyl oxygen. An intra-molecular hydrogen bond

between the N(3)-H(3) proton and O1 is present in ligands (**L1**-**L5**) [2.783-2.680 Å], creating a six-membered ring and favoring the Z-isomer with respect to the imine C=N bond. This hydrogen bond renders the isatin and TSc (N2-N3-C9/12/14/16-S1-N4) moieties essentially coplanar. The crystal structure of L1 showed the existence of an inter-molecular hydrogen bond between oxygen and water molecule [O(1W)–H(1WA)…O(1) = 2.846 Å]. Structure of **3** confirmed the square planar geometry of the complex. Complex **3** crystallized in triclinic *P*-1 space group with *Z* of 2. The Cu–S bond is longer than the Cu–Cl, Cu-O and Cu-N bonds [Cu(1)–S(1) 2.246 Å, Cu(1)–Cl(1) 2.179 Å, Cu(1)–O(1) 2.107 Å and Cu(1)–N(1) 1.974 Å], which are in the expected range for thiosemicarbazone complexes. The S1–C12 bond length (1.735 Å) in **3** is higher than that of L3 (1.670 Å). There is an increase in the C-O and C-N bond lengths (involved in coordination) in **3** compared to L3. The torsional angles in **3** are 3.66 [Cu(1)-S(1)-C(12)-N(2)], -176.96 [Cu(1)-S(1)-C(12)-N(4)], -173.00 [Cu(1)-O(1)-C(1)-N(3)].[37]

2.4. DNA binding studies

2.4.1. Electronic absorption titration

The electronic absorption spectrum of complex **1** exhibited two absorption bands at 336 and 427 nm which are assigned to ligand to metal charge transfer (LMCT) and d-d transition respectively. But in complexes **2**-**5**, only one band around 415-420 nm which corresponds to d-d transition. Hypochromism (Δε, 17-35%) with a small red shift around 3 nm was observed after the incremental addition of DNA to the complexes. Intercalative mode of binding due to the strong stacking interaction between an aromatic chromophore and the base pairs of DNA usually results in hypochromism along with or without a small red or blue shift.[38] The extent of shift and hypochromism correlate with the intercalative binding strength. The magnitude of hypochromism is in the order of **5**>**2**>**3**>**4**>**1**, which reflects the DNA binding efficacy of the complexes. The absorption spectra of the complexes (**1**-**5**) in the presence and absence of CT DNA are shown in Fig. 9. The binding constant of the complexes with CT DNA (K_b) was obtained from the ratio of slope to intercept in plots [DNA]/($\varepsilon_a - \varepsilon_f$) *versus* [DNA] according to the equation[39] [DNA]/($\varepsilon_a - \varepsilon_f$) = [DNA]/($\varepsilon_b - \varepsilon_f$) + 1/$K_b$ ($\varepsilon_b - \varepsilon_f$) where [DNA] is the concentration of DNA in base pairs, ε_a is the apparent extinction coefficient value found by calculating A(observed)/[complex], ε_f is the extinction coefficient for the free compound, and ε_b is the extinction coefficient for the compound in the fully bound form. Each set of data, when fitted into the above equation, gave a straight line

with a slope of $1/(\varepsilon_b - \varepsilon_f)$ and an y-intercept of $1/K_b(\varepsilon_b - \varepsilon_f)$ and the value of K_b was determined from the ratio of slope to intercept (Fig. 10). The magnitudes of intrinsic binding constants (K_b) are shown in Table 6. The observed values of K_b revealed that the Cu(II) complexes bind to DNA *via* intercalative mode.[40] The K_b values were found to be in the range of 1.06-2.09 × 10^4 M^{-1}. Complex **5** showed better DNA binding affinity compared to the other complexes. The presence of phenyl moiety in complex **5** may be the reason for its enhanced DNA binding ability. The results revealed that the binding constant are in the similar range for the other reported complexes.[41]

2.4.2. Viscosity measurements

Hydrodynamic method like viscosity measurements is a good technique to find out the binding of complexes to DNA. The values of relative specific viscosity (η/η^0), where η and η^0 are the specific viscosities of DNA in the presence and absence of the test complexes were determined and plotted against [complex]/[DNA]. Lengthening of DNA helix occurs on intercalation as base pairs are separated to accommodate the binding compound leading to increase in DNA viscosity. The increase in the viscosity of DNA follows the order **5** >**2**> **3**> **4** >**1**, but lower than that for the standard DNA intercalator EB. Thus, all these observations suggest that the N-substituted aromatic ring of complex **5** showed enhanced binding ability compared to other complexes.

2.4.3. Fluorescence spectroscopic studies

Fluorescence spectroscopic method is used to examine the binding modes of metal complexes with CT DNA. The Cu(II) complex show no fluorescence at room temperature in solution or in the presence of CT-DNA and their binding to DNA cannot be directly predicted through the emission spectra. Hence, competitive binding study was done to understand the mode of DNA interaction with the complexes.[42-44] Intense fluorescent light is emitted from EB in the presence of CT DNA due to its strong intercalation between adjacent DNA base pairs in the double helix; therefore, EB has been considered as a typical indicator of intercalation.[45] The changes observed in the spectra of CT DNA-EB are often used for the interaction study between DNA and metal complexes. If the metal complex intercalates into DNA, it leads to a decrease in the binding sites of DNA available for EB, resulting in decrease in the fluorescence intensity of the CT DNA-EB system. On adding Cu(II) complexes (0-50 μM) to CT DNA-EB, the quenching in the emission of DNA bound EB takes place (Fig. 12). Fluorescence quenching is explained by the Stern-Volmer equation[46] $F^o/F = 1 + K_q$ [Q] where F^o and F are the fluorescence intensities in the absence and presence of complex respectively, K_q is a linear Stern-Volmer quenching constant, and [Q] is the

concentration of complex. The slope of the plot of F^o/F *versus* [Q] gave K_q (Fig. 13). The apparent DNA binding constant (K_{app}) values was calculated by using the equation K_{EB} [EB] = K_{app} [complex] where [complex] is the complex concentration at 50% reduction in the fluorescence intensity of EB, $K_{EB} = 1.0 \times 10^7$ M^{-1} and [EB] = 5 µM. The quenching constant K_q and K_{app} values follows order **5>2>3>4>1,** which follows the same order as discussed in the absorption titration and values are listed in Table 6.

2.5. Protein binding studies

2.5.1. Absorbance and fluorescence studies

UV-Visible absorption titration of BSA with complexes (**1-5**) was done to predict the type of quenching process. Addition of the complex to BSA lead to an increase in BSA absorption intensity without affecting the position of absorption band. This indicates that the type of interaction between Cu(II) complexes and BSA was mainly a static quenching process.[47] The representative absorption titration spectra is shown in Fig. 14.

The binding studies of proteins with metal complexes were evaluated using fluorescence spectroscopy. Fig. 15 shows the fluorescence emission spectra of BSA and BSA after the addition of complexes (**1-5**). When increasing amount of complex solution was added to a fixed quantity of BSA, fluorescence intensity at 345 nm decreases upto 84.5, 90.9, 88.1, 87.7 and 91.9% for complexes **1-5** respectively, with hypsochromic shift of 7, 12, 10, 9 and 13 nm for complexes **1**, **2, 3, 4** and **5** respectively. The complexes interact hydrophobically with proteins which is evident from the observed hypochromism.[48] The fluorescence quenching is described by the Stern-Volmer relation $F^o/F = 1 + K_q$ [Q] where F^o and F demonstrate the fluorescence intensities in the absence and presence of quencher, respectively. K_q is a linear Stern-volmer quenching constant, and [Q] is the quencher concentration. The quenching constant (K_q) can be calculated using the plot of log (F^o/F) *versus* log [Q] (Fig. 16). When small molecules bind independently to a set of equivalent site, on a macromolecule, the equilibrium between free and bound molecules is represented by the Scatchard equation.[49, 50] $\log[(F^o - F)/F] = \log K_b + n \log[Q]$ where K_b is the binding constant of the complex with BSA and n is the number of binding sites. From the plot of $\log[(F^o - F)/F]$ *versus* log[Q] (Fig.17), the number of binding sites (n) and the binding constant (K_b) values have been obtained. The quenching constant (K_q), binding constant (K_b) and number of binding sites (n) for the interaction of the Cu(II) complexes with BSA are shown in Table 7. In all the complexes, only

one binding site is available to interact with BSA. Results showed that complexes **5** and **2** interact strongly with BSA compared to **3**, **4** and **1**.

2.5.2. Three-dimensional fluorescence spectroscopy analysis

It is well-known that three-dimensional fluorescence spectra can provide more detailed information about the changes in the configuration of proteins[51] which can be revealed from the changes in the contour map. Figure 18 represents the three-dimensional fluorescence spectra and contour map of BSA and BSA-complexes (**1-5**) in the absence and presence of complexes respectively. Peak a is the Rayleigh scattering peak and two typical fluorescence peaks (peak 1 and peak 2) also could be easily observed in three-dimensional fluorescence contour map of BSA with complexes. Among these two (peak 1 and peak 2), peak 2 mainly revealed the spectral characteristics of tryptophan and tyrosine residues. The reason is that when serum albumin is excited at 280 nm, it mainly reveals the intrinsic fluorescence of tryptophan and tyrosine residues. The excitation wavelength of peak 1 was noticed at 240 nm which was mainly attributed to the n–π^* transition of protein's characteristic polypeptide backbone structure, C=O.[52] The three-dimensional fluorescence contour map of BSA and BSA-complexes (**1-5**) was clearly different. From the fluorescence intensities of peak 2 decreased significantly in the presence of complexes (1–5) indicating the quenching of fluorescence of BSA by the complexes. The results shown in Table 9 indicated the conformational changes of BSA upon interaction with the complexes. The above phenomena and the analysis of the fluorescence characteristic of the peaks revealed that the binding complexes with BSA induced some micro-environmental and conformational changes in BSA.

2.5.3. Characteristics of synchronous fluorescence spectra

Synchronous fluorescence spectroscopy provides information about the molecular microenvironment, particularly in the vicinity of the fluorophore functional groups.[53] Tyrosine, tryptophan and phenylalanine residues are responsible for the fluorescence property of BSA. The difference between the excitation and emission wavelength ($\Delta\lambda$) reflects the nature of the chromophore.[54] The large $\Delta\lambda$ value, such as 60 nm, is characteristic of tryptophan residue and a small $\Delta\lambda$ value, such as 15 nm, is characteristic of tyrosine. The synchronous fluorescence spectra of BSA with various concentrations of Cu(II) complexes (**1-5**) were recorded at $\Delta\lambda$ = 15 nm and

$\Delta\lambda$ = 60 nm. On addition of the complexes, the fluorescence intensity of tryptophan residue at 340 nm decreased in the magnitude of 84.5, 91.63, 87.7, 86.9 and 92.7% for complexes **1**, **2**, **3**, **4** and **5** respectively (Fig. 19). Similarly, there was also decrease in the intensity of tyrosine residue at 300 nm. The magnitude of decrease was 61.5, 80.0, 74.2, 72.3 and 81.4% for complexes **1**-**5** respectively (Fig. 20). The synchronous fluorescence spectral studies clearly suggested that the fluorescence intensities of both the tryptophan and tyrosine were affected with increasing concentration of the complexes. The results indicate that the interaction of complexes with BSA affects the conformation of both tryptophan and tyrosine micro-region.[55]

2.6. DNA cleavage

The cleaving efficacy of complexes (**1-5**) has been assessed by their ability to convert supercoiled pUC19 DNA from form I to form II by agarose gel electrophoresis. As shown in (Fig 21), no distinct DNA cleavage was observed for the control in which the complex was absent (lane 1); however, with fixed concentration of the complexes (**1-5**), cleave SC (Form I) DNA into nicked circular (NC) (Form II) DNA, Hence, the complexes exhibited DNA cleavage activity in the absence of an external agent. Additionally, the amount of helical unwinding induced by the complex bound to SC DNA provides evidence for the intercalation mode of interaction between the complexes and DNA. The DNA cleavage activity of the complexes (**1-5**) can be estimated from the percentage of cleavage (C) (Table 8).

3. Conclusion

Five new copper(II) complexes with N-alkylated isatin based thiosemicarbazone ligands have been synthesized and characterized. Single crystal X-ray diffraction studies revealed that the Cu(II) complex have square planar geometry. The DNA binding affinity of the complexes were valuated using spectrophotometric methods. The results supported the interaction of the complexes with CT DNA through intercalation. Complexes **5** and **2** have better DNA cleaving ability compared to the other complexes. Fluorescence quenching experiments of BSA confirms the binding ability of the complexes and the mode of binding is static. In addition, the synchronous and 3D fluorescence spectral investigations revealed that the complexes induced a small change in the secondary structure of the protein at the studied conditions.

4. Experimental

4.1. Materials and methods

All the chemicals were purchased from Sigma Aldrich/Merck and used as received. Solvents were purified according to the standard procedures. The melting points were determined on Lab India instrument and are uncorrected. The elemental analyses were performed using a Vario EL−III CHNS analyzer. FT-IR spectra were recorded in the range of 4000-400 cm^{-1} (KBr pellets) and far-IR spectra were recorded in the range of 400-30 cm^{-1} (polyethylene pellets) using a PerkinElmer Frontier FT-IR/FIR spectrometer. UV-Visible spectra were recorded in the range of 900-250nm using a PG Instruments T90+UV-visible spectrophotometer in DMF solution. 3D fluorescence were measured on Horiba Scientific spectrofluorophotometer and Emission spectra were measured on a Jasco V-630 spectrophotometer using 5% DMF in buffer as the solvent. NMR spectra were recorded in $CDCl_3$ by using TMS as an internal standard on a Bruker 400 MHz spectrometer. EPR spectra were recorded on a JEOL EPR spectrometer at liquid nitrogen temperature, operating at X-band frequency (9.1 GHz).

4.2. Synthesis of ligands (L1- L5).

The indoline-2,3-dione based thiosemicarbazone ligands were synthesized using standard procedure.[56] Pyrrolidine-1-carbothiohydrazide and substituted indoline-2,3-dione were suspended in ethanol (20 mL) containing a few drops of glacial acetic acid added. The mixture was refluxed for 3 h and cooled to room temperature. The yellow product formed was filtered off, washed with cold ethanol and ether, and dried in vacuo. It was recrystallized from CH_3OH/C_2H_3N mixture (1:1) to get crystals of the title compounds.

4.2.1. N'-(2-oxoindolin-3-ylidene)pyrrolidine-1-carbothiohydrazide (L1)

Pyrrolidine-1-carbothiohydrazide (0.145 g, 0.001 mole), indoline-2,3-dione (0.147 g, 0.001 mole) were used. Yield: 82%. Yellow. m.p.: 151 ºC. Anal. Calc. for $C_{13}H_{14}N_4OS$ (%): C, 56.91; H, 5.14; N, 20.42; S, 11.69 Found: C, 56.45; H, 5.29; N, 20.53; S, 11.37. UV−Vis (CH_3OH): λ_{max}, nm (ε, $dm^3mol^{-1}cm^{-1}$) 278 (14000), 349 (25000). FT-IR (KBr): υ, cm^{-1} 3412, 3218 (H–N), 1676 (C=O), 1540 (C=N), 1285 (C=S). ^1H NMR (400 MHz, $CDCl_3$): δ, ppm 13.33 (s, 1H),

7.80-7.78 (d, *J* = 8.0 Hz, 1H), 7.33-7.31 (t, *J* = 8.0 Hz, 1H), 7.29-7.26 (t, *J* = 8.0 Hz, 1H), 7.24-7.09 (m, *J* = 8.0 Hz, 1H), 6.90-6.88 (d, *J* = 8.0 Hz, 1H), 4.01-3.98 (t, *J* = 4.0 Hz, 2H). 3.73-3.70 (t, *J* = 8.0 Hz, 2H), 2.17-2.10 (m, 2H), 2.027-1.97 (m, 2H). ^{13}C NMR (100 MHz, $CDCl_3$): δ, ppm 176.2 (C=S), 162.7 (C=O), 139.7 (C=N), 130.7, 129.0, 128.2, 123.3, 121.8, 110.5 (aromatic C), 29.7, 28.9, 26.4, 24.2 (aliphatic C). ESI-MS m/z=274.18 $[M]^+$.

4.2.2. N'-(2-oxo-1-(prop-2-yn-1-yl)indolin-3-ylidene)pyrrolidine-1-carbothiohydrazide (L2)

Pyrrolidine-1-carbothiohydrazide (0.145 g, 0.001 mole), 1-(prop-2-yn-1-yl)indoline-2,3-dione (0.185 g, 0.001 mole) were used. Yield: 79%. Yellow. m.p.: 167 °C. Anal. Calc. $C_{16}H_{16}N_4OS$ (%): C, 61.52; H, 5.16; N, 17.93; S, 10.26. Found: C, 61.12; H, 5.28; N, 17.65; S, 10.41. UV−Vis (CH_3OH): λ_{max}, nm (ε, $dm^3mol^{-1}cm^{-1}$) 282 (17000), 350 (29500). FT-IR (KBr): υ, cm^{-1} 3184 (N–H), 1689 (C=O), 1578 (C=N), 1276 (C=S). ^{1}H NMR (400 MHz, $CDCl_3$): δ, ppm 13.36 (s, 1H), 7.86-7.84 (d, *J* = 8.0 Hz, 1H), 7.42-7.38 (t, *J* = 8.0 Hz, 1H), 7.19-7.09 (m, 1H), 4.57-4.56 (d, *J* = 4.0 Hz, 2H), 4.01-3.98 (t, *J* = 8.0 Hz, 2H), 3.75-3.72 (t, *J* = 4.0 Hz, 2H), 2.30-2.13 (m, 3H), 2.0-1.98 (m, 2H). ^{13}C NMR (100 MHz, $CDCl_3$): δ, ppm 176.3 (C=S), 160.8 (C=O), 140.8 (C=N), 130.6, 123.7, 121.6, 120.0, 109.6 (aromatic C), 30.9, 28.9, 26.4, 24.2 (aliphatic C). ESI-MS m/z=312.58 $[M+1]^+$.

4.2.3. N'-(1-allyl-2-oxoindolin-3-ylidene)pyrrolidine-1-carbothiohydrazide (L3)

Pyrrolidine-1-carbothiohydrazide (0.145 g, 0.001 mole), 1-allylindoline-2,3-dione (0.187 g, 0.001 mole) were used. Yield: 89%. Yellow. m.p.: 160 °C. Anal. Calc. for $C_{16}H_{18}N_4OS$ (%): C, 61.12; H, 5.77; N, 17.82; S, 10.20. Found: C, 60.90; H, 5.93; N, 17.66; O, S, 9.74. UV−Vis (CH_3OH): λ_{max}, nm (ε, $dm^3mol^{-1}cm^{-1}$) 280 (15500), 351 (26000). FT-IR (KBr): υ, cm^{-1} 3222 (N–H), 1682 (C=O), 1547 (C=N), 1276 (C=S). ^{1}H NMR (400 MHz, $CDCl_3$): δ, ppm 13.48 (s, 1H), 7.83-7.81 (d, *J* = 8.0 Hz, 1H), 7.35-7.29 (q, *J* = 8.0 Hz, 1H), 7.14-7.10 (t, *J* = 8.0 Hz, 1H), 6.89-6.87 (d, *J* = 8.0 Hz, 1H), 5.91-5.81(m, 1H), 4.40-4.39 (d, *J* = 4.0 Hz, 2H), 4.00-3.97 (t, *J* = 4, 2H), 3.73-3.70 (t, *J* = 8.0 Hz, 2H), 2.17-2.10 (m, 2H), 2.0-1.97 (m, 2H). ^{13}C NMR (100 MHz, $CDCl_3$): δ, ppm 176.3 (C=S), 161.4 (C=O), 141.8 (C=N), 134.0, 130.5, 123.3, 121.5, 119.9, 118.1, 109.6 (aromatic C), 53.2, 48.9, 41.9, 30.9, 26.3, 24.20 (aliphatic C). ESI-MS m/z=314.56 $[M+1]^+$.

4.2.4. N'-(2-oxo-1-pentylindolin-3-ylidene)pyrrolidine-1-carbothiohydrazide (L4)

Pyrrolidine-1-carbothiohydrazide (0.145 g, 0.001 mole), 1-pentylindoline-2,3-dione (0.217 g, 0.001 mole) were used. Yield: 90%. Yellow. m.p.: 149 °C. Anal. Calc. $C_{18}H_{24}N_4OS$ (%): C, 62.76; H, 7.02; N, 4.64; S, 9.31. Found: C, 62.25; H, 7.51; N, 16.08; S, 9.72. UV−Vis (CH_3OH):

λ_{max}, nm (ε, $dm^3mol^{-1}cm^{-1}$) 281 (16000), 350 (24500). FT- FT-IR (KBr): υ, cm^{-1} 3167 (N–H), 1686 (C=O), 1577 (C=N), 1274 (C=S). ^{1}H NMR (400 MHz, $CDCl_3$): δ, ppm 13.51 (s, 1H), 7.84-7.83 (d, *J* = 8.0 Hz, 2H), 7.41-7.38 (t, *J* = 8.0 Hz, 1H), 7.19-7.09 (m, 1H), 4.01-3.98 (t, *J* = 8.0 Hz, 2H), 3.76- 3.72 (t, *J* = 8.0 Hz, 2H), 3.71-3.68 (m, *J* = 4.0 Hz, 2H), 2.30-2.13 (m, 2H), 2.0-1.98 (m, 2H), 1.71-1.61 (m, 4H), 1.43-1.34 (m, 2H), 0.98- 0.96 (m, *J* = 8.0 Hz, 3H). ^{13}C NMR (100 MHz, $CDCl_3$): δ, ppm 176.3 (C=S), 161.7 (C=O), 141.8 (C=N), 134.1, 130.5, 128.8, 123.2, 121.5, 109.8 (aromatic C), 39.6, 30.6, 29.7, 28.9, 26.4, 24.2, 20.2, 13.7 (aliphatic C). ESI-MS m/z=344.81 $[M+1]^+$.

4.2.5. N'-(1-benzyl-2-oxoindolin-3-ylidene)pyrrolidine-1-carbothiohydrazide (L5)

Pyrrolidine-1-carbothiohydrazide (0.145 g, 0.001 mole), 1-benzylindoline-2,3-dione (0.237 g, 0.001 mole) were used. Yield: 81%. Yellow. m.p.: 171 ºC. Anal. Calc. $C_{20}H_{20}N_4OS$ (%): C, 65.91; H, 5.53; N, 15.37; S, 8.80. Found: C, 65.47; H, 5.32; N, 15.64; S, 8.59. UV−Vis (CH_3OH): λ_{max}, nm (ε, $dm^3mol^{-1}cm^{-1}$) 279 (19000), 351 (33500). FT-IR (KBr): υ, cm^{-1} 3187 (N–H), 1689 (C=O), 1582 (C=N), 1251 (C=S). ^{1}H NMR (400 MHz, $CDCl_3$): δ, ppm 13.50 (s, 1H), 7.84-7.83 (d, *J* = 4.0 Hz, 1H), 7.42-7.38 (t, *J* = 8.0 Hz, 1H), 7.35-7.23 (m, 6H), 7.10-7.07 (t, *J* = 4.0 Hz , 1H), 6.79-6.77 (d, *J* = 4.0 Hz , 1H), 4.96 (s. 2H), 4.00-3.96 (t, *J* = 8.0 Hz, 2H), 3.74-3.72 (t, *J* = 4.0 Hz, 2H), 2.29-2.11 (m, 2H), 2.0-1.97 (m, 2H). ^{13}C NMR (100 MHz, $CDCl_3$): δ, ppm 176.4 (C=S), 161.7 (C=O), 141.9 (C=N), 134.9, 134.0, 130.5, 128.9, 128.0, 127.2, 123.4, 121.5, 120.0, 109.8 (aromatic C), 53.0, 50.7. 49.03. 26.4, 24.2 (aliphatic C). ESI-MS m/z=364.20 $[M+]^+$.

4.3. Synthesis of copper (II) complexes (1-5)

The chloroformic solution of $CuCl_2.2H_2O$ (1 mmol) was added into the solution of an appropriate substituted isatin thiosemicarbazone ligands (1 mmol) in methanol. The reaction mixture was stirred for 30 min at room temputure, and then the precipitate formed was filtered and washed with chloroform. The suitable crystals for X-ray diffraction were grown from CH_3OH/C_2H_3N mixture (1:1).

4.3.1. N'-(2-oxoindolin-3-ylidene)pyrrolidine-1-carbothiohydrazide copper(II) (1)

$CuCl_2.2H_2O$ (0.170 g, 0.001 mole), L1 (0.274 g, 0.001 mole) were used. Yield: 79%. Light brown block solid. m.p.: 233 °C. Anal. Calcd. For $C_{13}H_{13}ClCuN_4OS$: C, 41.94; H, 3.52; N, 15.05; S, 8.61. Found: C, 41.61; H, 3.74; N, 15.23; S, 8.56. UV−Vis (DMF): λ_{max}, nm (ε, $dm^3mol^{-1}cm^{-1}$) 272 (4333), 380 (8000), 429 (9666). FT-IR (KBr): υ, cm^{-1} 3408 (N–H), 1612 (C=O), 1497 (C=N),

1230 (C= S) and far-IR (Polyethylene) υ, cm^{-1} 388 (Cu–N_{azo}), 340 (Cu-S), 312 (Cu-Cl). ESI-MS m/z=373.57 $[M + 1]^+$. Epr (LNT): 'g' values 2.238, 2.052

4.3.2. N'-(2-oxo-1-(prop-2-yn-1-yl)indolin-3-ylidene)pyrrolidine-1-carbothiohydrazide) copper(II) (2)

$CuCl_2.2H_2O$ (0.654 g, 0.001 mole), L2 (0.312 g, 1 0.001 mole) were used. Yield: 82%. Light brown block solid. m.p.: 241 °C; Anal. Calcd. for $C_{16}H_{15}ClCuN_4OS$: C, 46.83; H, 3.68; N, 13.65; S, 7.81. Found: C, 46.61; H, 3.71; N, 13.43; S, 7.60. UV−Vis (DMF): λ_{max}, nm (ε, $dm^3mol^{-1}cm^{-1}$) 273 (9333), 374 (10000), 420 (11666). FT-IR (KBr): υ, cm^{-1} 1600 (C=O), 1514 (C=N), 1201 (C= S) and far-IR (Polyethylene) υ, cm^{-1} 399 (Cu–N_{azo}), 336 (Cu-S), 311(Cu-Cl). ESI-MS m/z=410.07 $[M]^+$. Epr (LNT): 'g' values 2.240, 2.064.

4.3.3. N'-(1-allyl-2-oxoindolin-3-ylidene)pyrrolidine-1-carbothiohydrazide) copper(II) (3)

$CuCl_2.2H_2O$ (0.170 g, 0.001 mole), L3 (0.314 g, 0.001 mole) were used. Yield: 79%. Light brown block solid. m.p.: 246 °C. Anal. Calcd. For $C_{16}H_{17}ClCuN_4OS$: C, 46.60; H, 4.15; N, 13.59; S, 7.78. Found: C, C, 46.43; H, 4.01; N, 13.19; S, 7.91. UV−Vis (DMF): λ_{max}, nm (ε, $dm^3mol^{-1}cm^{-1}$) 269 (12666), 376 (19000), 428 (24000). FT-IR (KBR): υ, cm^{-1} 1600 (C=O), 1507 (C=N), 1192 (C= S) and far-IR (Polyethylene): υ, cm^{-1} 397 (Cu–N_{azo}), 349 (Cu-S), 317 (Cu-Cl). ESI-MS m/z=412.10 $[M]^+$. Epr (LNT): 'g' values 2.215, 2.031.

4.3.4. N'-(2-oxo-1-pentylindolin-3-ylidene)pyrrolidine-1-carbothiohydrazide copper(II) (4)

$CuCl_2.2H_2O$ (0.170 g, 0.001 mole), L4 (0.344 g, 0.001 mole) were used. Yield: 80%; Light brown block solid. m.p.: 233 °C. Anal. Calcd. for $C_{18}H_{23}ClCuN_4OS$: C, 48.86; H, 5.24; N, 12.66; S, 7.25. Found: C, 48.59; H, 5.11; N, 12.93; S, 7.20 UV−Vis (DMF): λ_{max}, nm (ε, $dm^3mol^{-1}cm^{-1}$) 271 (11666), 373 (17333), 417 (23666). FT-IR (KBr): υ, cm^{-1}1646 (C=O), 1510 (C=N), 1183 (C= S) and far-IR (Polyethylene): υ, cm^{-1} 398 (Cu–N_{azo}), 326 (Cu-S), 319 (Cu-Cl). ESI-MS m/z=442.09 $[M]^+$. Epr (LNT): 'g' values 2.207, 2.063.

4.3.5. N'-(1-benzyl-2-oxoindolin-3-ylidene)pyrrolidine-1-carbothiohydrazide) copper(II) (5)

$CuCl_2.2H_2O$ (0.170 g, 0.001 mole), L5 (0.364 g, 0.001 mole) were used. Yield: 76%. Light brown block solid. m.p.: 255 °C. Anal. Calcd. for $C_{20}H_{29}ClCuN_4OS$: C, 51.94; H, 4.14; N, 12.12; S, 6.93. Found: C, 51.99; H, 4.30; N, 12.00; S, 6.72. UV−Vis (DMF): λ_{max}, nm (ε, $dm^3mol^{-1}cm^{-1}$) 270 (10333), 382 (16000), 427 (21666). FT-IR (KBr): υ, cm^{-1} 1603 (C=O), 1514 (C=N), 1166 (C= S) and far-IR (Polyethylene): υ, cm^{-1} 392 (Cu–N_{azo}), 334 (Cu-S), 308 (Cu-Cl). ESI-MS m/z=463.13 $[M + 1]^+$. Epr (LNT): 'g' values 2.216, 2.046.

4.4. Single crystal X-ray diffraction studies

A Bruker APEX2 X-ray (three-circle) diffractometer was employed for crystal screening, unit cell determination, and data collection. The X-ray radiation employed was generated from a Mo sealed X-ray tube (K_α = 0.70173 Å with a potential of 40 kV and a current of 40 mA) fitted with a graphite monochromator in the parallel mode (175 mm collimator with 0.5 mm pinholes). Sixty data frames were taken at widths of 0.5°. These reflections were used in the auto-indexing procedure to determine the unit cell. A suitable cell was found and refined by nonlinear least squares and Bravais lattice procedures. The unit cell was verified by examination of the *h k l* overlays on several frames of data by comparing with both the orientation matrices. No super-cell or erroneous reflections were observed. After careful examination of the unit cell, a standard data collection procedure was initiated using omega scans. Integrated intensity information for each reflection was obtained by reduction of the data frames with the program APEX2.[57] The integration method employed a three dimensional profiling algorithm and all data were corrected for Lorentz and polarization factors, as well as for crystal decay effects. Finally, the data were merged and scaled to produce a suitable data set. The absorption correction program SADABS [58] was employed to correct the data for absorption effects. Systematic reflection conditions and statistical tests of the data suggested the space group. Solution was obtained readily using XT/XS in APEX2 .[59] Hydrogen atoms were placed in idealized positions and were set riding on the respective parent atoms. All non-hydrogen atoms were refined with anisotropic thermal parameters. The structure was refined (weighted least squares refinement on F^2) to convergence.[60] Olex2 was employed for the final data presentation and structure plots.[59]

4.5. DNA binding studies

The binding of metal complexes with CT DNA was carried out in Tris HCl/NaCl buffer (pH 7.2). The bulk solution of CT DNA was prepared by diluting the CT DNA using Tris HCl/NaCl buffer followed by stirring at 4 °C for three days, and kept at 4 °C for not more than a week. The stock solution of CT DNA gave a ratio of UV absorbance at 260 and 280 nm (A260/A280) of 1.9, indicating that the DNA was sufficiently free of proteins. The bulk DNA solution was further diluted to 10 folds to show maximum absorbance at 260 nm. The absorption coefficient of CT DNA was 6600 cm^{-1} M^{-1} per nucleotide.[61] Cu(II) complexes of required concentration were prepared by dissolving the calculated amount of the complexes in 5% DMF/Tris HCl/NaCl. Complex solution of concentration 15 µM was taken in cuvette and CT DNA

of equivalent concentration (5–40 μM) was added each time and the significant absorbance change was noted.

The competitive binding of each complex with EB has been investigated by fluorescence spectroscopic technique in order to examine whether the complex can displace EB from its CT DNA-EB complex. Ethidium bromide solution was prepared using Tris HCl/NaCl buffer (pH 7.2). The test solution was added in aliquots of 2.5 μM concentration to DNA-EB and the change in fluorescence intensities at 596 nm (450 nm excitation) was noted down.

Viscosity experiments were carried out using a semi micro viscometer maintained at 27 °C in a thermostatic water bath. DNA samples (0.5 μM) were prepared by sonication in order to minimize complexities arising from DNA flexibility. Flow time was measured three times for each sample and an average flow time was calculated. The values of relative specific viscosity (η/η^0), where η is the relative viscosity of DNA in the presence of the complex and η0 is the relative viscosity of DNA alone, were plotted against 1/R (1/R = [compound]/[DNA]). Relative viscosity (η^0) values were calculated from the observed flow time of the DNA solution (t) corrected for the flow time of the buffer alone (t^0), using the expression $\eta^0 = (t - t^0)/t^0$.

4.6. Protein binding studies

The binding of Cu(II) complexes (**1**-**5**) with BSA was studied using fluorescence spectra recorded at a fixed excitation wavelength corresponding to BSA at 280 nm and monitoring the emission at 335 nm. The excitation and emission slit widths and scan rates were constantly maintained for all the experiments. Stock solution of BSA was prepared in 50 mM phosphate buffer (pH = 7.2) and stored in the dark at 4 °C for further use. Concentrated stock solutions of each test compound were prepared by dissolving them in DMF–phosphate buffer (5:95) and diluted with phosphate buffer to get required concentrations. 2.5 ml of BSA solution was titrated by successive additions of a 10^{-6} M stock solution of the complexes using a micropipette. For synchronous fluorescence spectra measurements, the same concentration of BSA and the complexes were used and the spectra were measured at two different Δλ (difference between the excitation and emission wavelengths of BSA) values of 15 and 60 nm.

In three dimensional fluorescence studies, the emission wavelength was recorded between 240 and 440 nm, and the excitation wavelength was recorded from 200 to 360 nm at 10 nm increments. The other scanning parameters were just the same as the fluorescence quenching experiments.[62]

4.7. DNA cleavage studies

A mixture of Tris buffer (5mMTris–HCl/50mMNaCl buffer, pH7.2), pUC19 plasmid DNA (150 µg mL^{-1}) and different amounts of the complexes (1–5) were incubated for 3 h at 37 ^{o}C. A dye solution (0.05% bromophenol blue and 5% glycerol) was added to the mixture prior to electrophoresis. The samples were then analyzed by 1.5% agarose gel electrophoresis [Tris–HCl/boric acid/EDTA (TBE) buffer, pH 8.0] for 2 h at 60 mV. The gel was stained with 0.5 µg mL^{-1} ethidium bromide, visualized by UV light and photographed. The extent of cleavage of pUC19 was determined by measuring the intensity of the bands using AlphaImager HP instrument.

References

1 B. Rosenberg, L. VamCamp, J. E. Trosko and V. H. Mansour, *Nature.*, 1969, **222**, 385- 386.

2 O. Zelenko, J. Gallagher, Y. Xu, D.S. Sigman, *Inorg. Chem.*, 1998, **37**, 2198-2204.

3 Z. Wu, Q. Liu, X. Liang, X. Yang, N. Wang, X. Wang, H. Sun, Y. Lu and Z. Guo, *J. Inorg. Biochem.*, 2009, **14**, 1413-1323.

4 D. Senthil Raja, N. S. P. Bhuvanesh and K. Natarajan, *Dalton Trans.*, 2012, **41**, 4365−4377.

5 X. Qiao, Z. Y. Ma, C. Z. Xie, F. Xue, Y. W. Zhang, J. Y. Xu, Z. Y. Qiang, J. S. Lou, G.J.Chen, S.P.Yan, *J. Inorg. Biochem.*, 2011, **105**, 728–737.

6 P. J. Bednarski, F. S. Mackay and P. J. Sadler, Anticancer Agents *Med. Chem.*, 2007, **7**, 75-93.

7 A. T. Chaviara, P. C. Christidis, A. Papageorgiou, E. Chrysogelou, D. J. Hadjipavlou-Litina and C. A. Bolos, *J. Inorg. Biochem.*, 2005, **99,** 2102-2109.

8 T. Fujimori, S. Yamada, H. Yasui, H. Sakurai, Y. In and T. J. Ishida, *J. Inorg. Biochem.*, 2005, **10**, 831-841.

9 F. L. Yin, J. Shen, J. J. Zou and R. C. Li, *Acta Chim. Sinica.*, 2003, **61,** 556-561.

10 P. M. May, D. R. Williams, *In Metal Ions in Biological Systems*, H. Sigel, Ed., Marcel Dekker, New York. 1981, **101**, 283–317.

11 T. Miura, A. Hori-i, H. Mototani and H. Takeuchi, *Biochemistry.*, 1999, **38,** 11560–11569.

12 C. Fernandes, G. L. Parrilha, J. A. Lessa, L. J. M. Santiago, M. M. Kanashiro, F. S. Boniolo, A. J. Bortoluzzi, N. V. Vugman, M. H. Herbst and A. Horn Jr, *Inorg. Chim. Acta.*, 2006, **359,** 3167–3176.

13 B. C. Bales, T. Kodama, Y. N. Weledji, M. Pitie, B. Meunier and M. M. Greenberg, *Nucl. Acid Res.*, 2005, **33,** 5371–5379.

14 P. K. M. Siu, D. L. Ma and C. M. Che, *Chem. Commun.*, 2005, 1025-1027.

15 J. N. Tian, J. Q. Liu, X. Tian, Z. D. Hu and X. G. Chen, *J. Mol. Struct.*, 2004, **691**, 197-202.

16 J. Seetharamappa and B. P. Kamat, *Chem. Pharm. Bull.*, 2004, **52,** 1053-1057.

17 (a) S. B. Padhye and G. B. Kauffman, *Coord. Chem. Rev.*, 1985, **63**, 127–160 (b) I. Haiduc

and C. Silvestru, *Coord. Chem. Rev.*, 1990, **99**, 253–296 (c) D. X. West, S. B. Padhye and P. B. Sonawane, *Struct. Bonding.*, 1991, 76, 1–50 (d) D. X. West, A. E. Liberta, S. B. Padhye, R. C. Chikate, P. B. Sonawane, A. S. Kumbhar and R. G. Yerande, *Coord. Chem. Rev.*, 1933, 123, 49–71.

18 Y. P. Tion, C. Y. Duan, Z. L. Lu, X. Z. You, H. K. Fun and S. Kandasamy, *Polyhedron.*, 1996, **15**, 2263–2271.

19 (a) P. Souza, I. A. Matesanz and V. J. Fernandez, *Dalton Trans.*, 1996, **6,** 3011–3013 (b) D. Kovala-Demertzi, A. Domopoulou, M. A. Demertzis, J. Valdes-Martinez, S. Hernandez-Ortega, G. Espinosa- Perez, D. X. West, M. M. Salberg, G. A. Bain and P. D. Bloom, *Polyhedron.*, 1996, **15,** 2587–2596 (c) M. A. Ali, K. K. Dey, M. Nazimuddin, F. E. Smith, R. J. Butcher, J. P. Jasinski and J. M. Jasinski, *Polyhedron.*, 1996, **15**, 3331–3339.

20 Rohith P. John, A. Sreekanth, Maliyeckal R. Prathapachandra Kurup, Anwar Usman, Abdul Razak Ibrahim, Hoong-Kun Fun, *Spectrochimica Acta part A.*, 2003, **59**, 1349-1358.

21 J.P. Scovill, D.L. Klayman, C.F. Franchino, *J. Med. Chem.*, 1982, **25,** 1261.

22 D.L. Klayman, J.P. Scovill, J.F. Bartosevich, C.J. Mason, *J. Med. Chem.*, 1979, **22,** 1367.

23 D.L. Klayman, J.F. Bartosevich, T.S. Griffin, C.J. Mason, J.P. Scovill, *J. Med. Chem.*, 1979, **22**, 855.

24 I.H. Hall, K.G. Rajendran, D.X. West, A.E. Liberta, *Anticancer drugs.*, 1993, **4**, 251.

25 P. Genova, T. Varadinova, A.I. Matesanz, D. Marinova, P. Souza, *Toxicol. Appl.Pharmacol.*, 2004, **197**, 107.

26 U. Abram, K. Ortner, K. Sommer, J. Chem. Soc., *Dalton Trans.*, (1999) 735.

27 R. Dimmer, U. Dittes, B. Nuber, V. Sefried, W. Opferkuch, B.K. Keppler, *Metal Based Drugs.*, 1995, **2**, 271.

28 D.X. West, G.A. Bain, R.J. Butcher, J.P. Jasinski, Y. Li, R.Y. Pozdniakiv, J. Valdes-Martinez,R.A. Toscano, S. Hernandes-Ortega, *Polyhedron.*, 1996, **15**, 665.

29 D. Kovala-Demertzi, A. Domopoulou, M. Demertzis, C.P. Paptopoulou, A. Terzis, *Polyhedron.*, 1994, **13**, 1917.

30 Z. Afrasiabi, E. Sinn, J. Chen, Y. Ma, A.L. Rheingold, L.N. Zakharov. N. Rath, S. Padhye, *Inorg. Chim. Acta.*, 2004, **357**, 271.

31 (a) West, D. X. Padhye, S. B. Sonaware, P. B. *Struct. Bonding (Berlin).*, 1991, **76**, 4. (b)

West, D. X. Liberta, A. E.; Padhye, S. B. Chilate, R. C. Sonaware, P. B. Kumbhar, A. S. Yerande, R. G. *Coord. Chem. ReV.*, 1993, **123**, 49.

32 (a) Liberta, A. E. West, D. X. Biometals 5 (2005) 21. (b) Joseph, M.; Kuriakose, M. Kurup, M. R. P. Suresh, E. Bhat, S. G. *Polyhedron.*, 2006, **25**, 61. (c) Padhye, S. Chikate, R. Kumbhar, A. Shallon, J. M. Chitnis, M. P. *Biometals.*, 1992, **5**, 67.

33 Anantharam Sreekanth, Maliyeckal R. Prathapachandra Kurup, *Polyhedron.*, 2003, **20** 3321–3332.

34 R. Prabhakaran, R. Sivasamy, J. Angayarkanni, R. Huang, P. Kalaivani, R. Karvembu, F. Dallemer and K. Natarajan, *Inorg. Chim. Acta.*, 2011, **374**, 647–653.

35 S. S. Batsanov, *J. Mol. Struct.*, 2011, **990**, 63-66.

36 B. Cordero, V. Gomez, A. E. Platero-Prats, M. Reves, J. Echeverria, E. Cremades, F. Barragan, S. Alvarez, *Dalton Trans.*, 2008, 2832-2838.

37 Jebiti Haribabu, Kumaramangalam Jeyalakshmi, Yuvaraj Arun, Nattamai S. P. Bhuvanesh, Paramasivan Thirumalai Perumal and Ramasamy Karvembu, RSC Adv. 4 (2014) 17179-17195

38 J. S. Guerrero, P. C. Sanchez, E. R. Perez, F. V. Garcia, M. E. B. Gomez and L. R. Azuara, *Toxicol. in Vitro.*, 2011, **25**, 1376 -1384.

39 A. M. Pyle, J. P. Rehmann, R. Meshoyrer, C. V. Kumar, N. J. Turro and J. K. Barton, *J. Am.Chem. Soc.*, 1989, **111**, 3051–3058.

40 A. Wolf, G. H. Shimer and T. Meehan, *Biochemistry.*, 1987, **26**, 6392–6396.

41 Monica Baldini, Marisa Belicchi-Ferrari, Franco Bisceglie, Giorgio Pelosi, Silvana Pinelli and Pieralberto Tarasconi *J. Inorg. Biochem.*, 2013, 42, 2049-2055.

42 N. Chitrapriya, T. Sathiya Kamatchi, M. Zeller, H. Lee and K. Natarajan, *Spectrochim. Acta, Part A.*, 2011, **81**, 128–134.

43 J. R. Lakowicz and G. Webber, *Biochemistry.*, 1973, **12,** 4161– 4170.

44 B. C. Baguley and M. Lebret, *Biochemistry.*, 1984, **23**, 937–943.

45 W. D. Wilson, L. Ratmeyer, M. Zhao, L. Strekowski and D. Boykin, *Biochemistry.*, 32 1993, **32**, 4098–4104.

46 K. S. Ghosh, B. K. Sahoo, D. Jana and S. Dasgupta, *J. Inorg. Biochem.*, 2008, **102**, 1711–1718.

47 D. Senthil Raja, G. Paramaguru, N. S. P. Bhuvanesh, J. H. Reibenspies, R. Renganathan and K. Natarajan, *Dalton Trans.,* 2011, 4548–4559.

48 D. Senthil Raja, N. S. P. Bhuvanesh and K. Natarajan, *Eur. J. Med. Chem.*, 2011, **46**, 4584 4594.

49 J. R. Lakowicz, Fluorescence Quenching: Theory and Applications. *Principles of Fluorescence Spectroscopy,* Kluwer Academic/Plenum Publishers, New York 1999, 53–127.

50 X. Z. Feng, Z. Yang, L. J. Wang and C. Bai, *Talanta.,* 1998, **47**, 1223–1229.

51 G. Z. Chen, X. Z. Huang, Z. Z. Zheng, J. G. Xu and Z. B. Wang, *Analysis Method of Fluorescence*, Science Press, Beijing, 3rdedn, 1990.

52 J. N. Miller, *Proc. Anal. Div. Chem. Soc.,* 1979, **16,** 203–208.

53 P. Krishnamoorthy, P. Sathyadevi, A. H. Cowley, R. R. Butorac and N. Dharmaraj, *Eur. J. Med. Chem.,* 2011, **46,** 3376–3387.

54 G. W. Zhang, Q. M. Que, J. H. Pan and J. B. Guo, *J. Mol. Struct.,* 2008, **881**, 132–138.

55 A. N. Glazer and E. L. Smith, *J. Biol. Chem.,* 1961, **236**, 2942–2947.

56 J. Zhou, D. Wu and D. Guo, *J. Chem. Technol. Biotechnol.,* 2010, **85**, 1402–1406.

57 APEX2, *Program for Data Collection on Area Detectors*, BRUKER AXS Inc., 5465 East Cheryl Parkway, Madison, WI 53711–5373, USA.

58 Sheldrick, G.M. "Program for Absorption Correction of Area Detector Frames", BRUKER AXS Inc., 5465 East Cheryl Parkway, Madison, WI 53711-5373 USA

59 G. M. Sheldrick, *Acta Crystallogr. Sect. A: Found. Crystallogr.,* 64 (2008) 112–122.

60 O. V. Dolomanov, L. J. Bourhis, R. J. Gildea, J. A. K. Howard and H. Puschmann, *J. Appl. Crystallogr.,* 2009, **42**, 339–341.

61 M. E. Reichmann, S. A. Rice and P. Thomas, *J. Am. Chem. Soc.,* 1954, **76**, 3047–3053.

62 P. Kalaivani, R. Prabhakaran, E. Vaishnavi, T. Rueffer, H. Lang, P. Poornima, R. Renganathan, V. V. Padma and K. Natarajan, *Inorg. Chem. Front.,* 2014, **1,** 311–324.

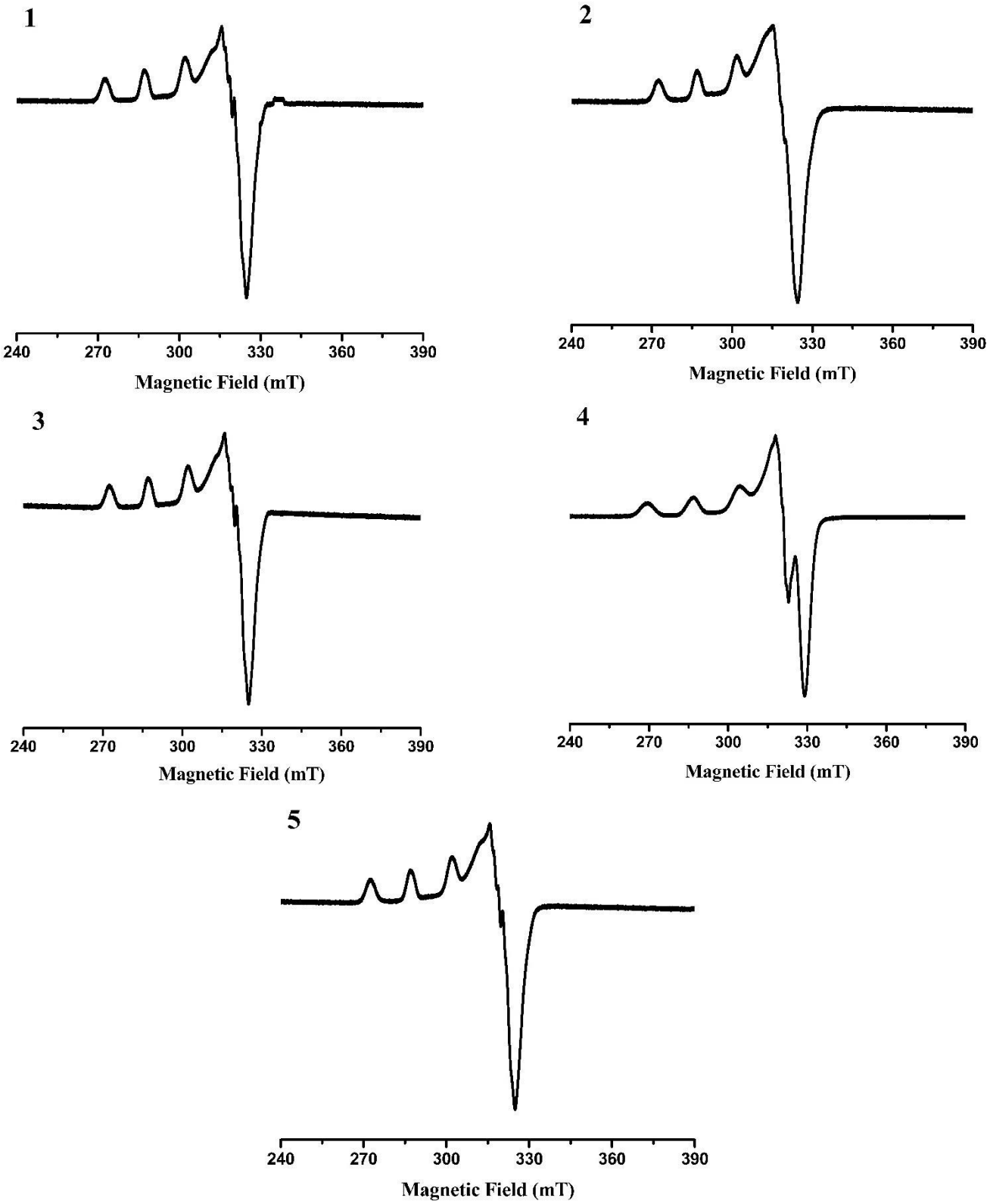

Fig. 2 EPR spectrum of complexes in frozen DMF solution. Microwave power, 0.98 mW; microwave frequency, 9.1 GHz.

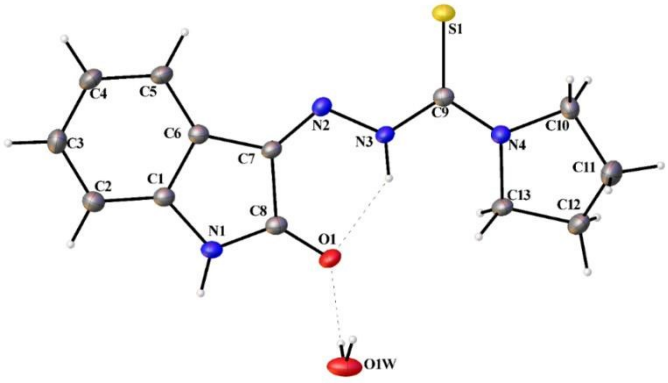

Fig. 3 The molecular structure of complex **L1**, with displacement ellipsoids drawn at the 50% probability level.

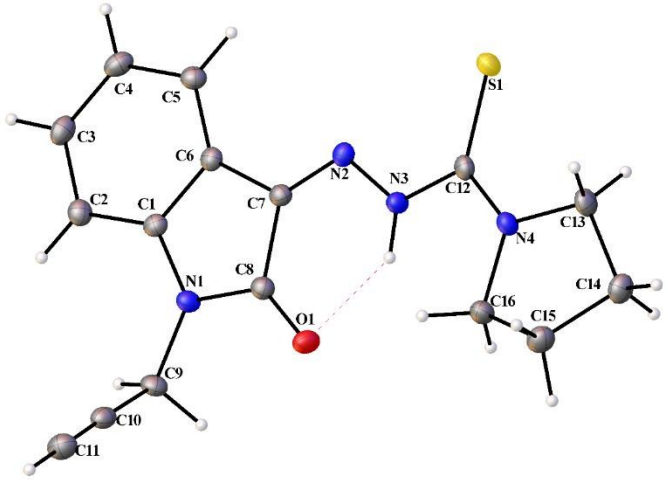

Fig. 4 The molecular structure of complex **L2**, with displacement ellipsoids drawn at the 50% probability level

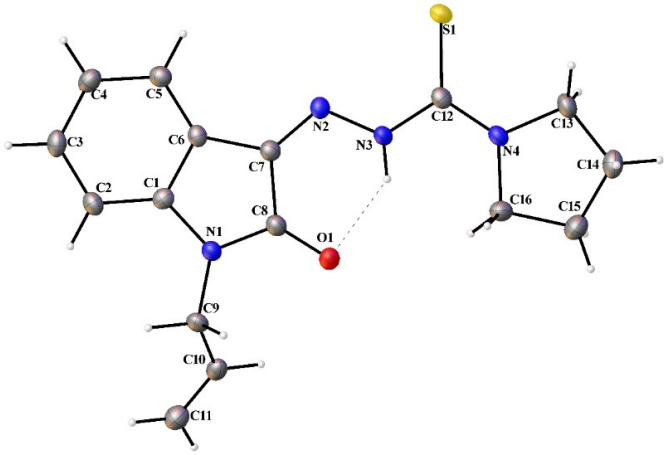

Fig. 5 The molecular structure of complex **L3**, with displacement ellipsoids drawn at the 50% probability level

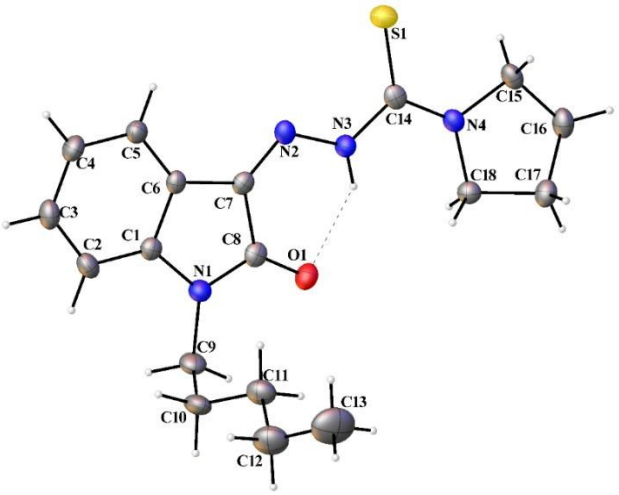

Fig. 6 The molecular structure of complex **L4**, with displacement ellipsoids drawn at the 50% probability level

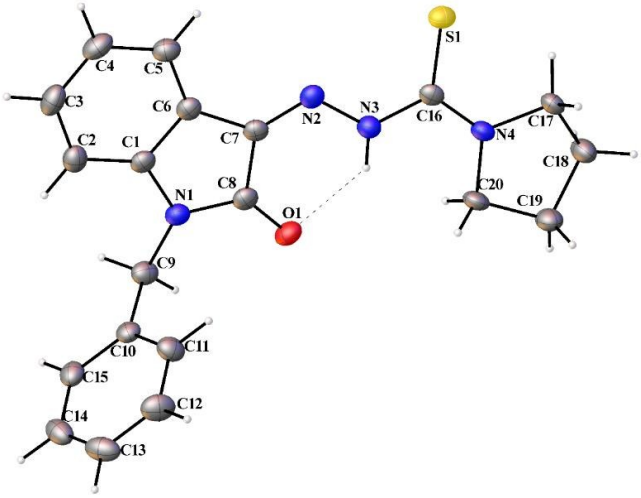

Fig. 7 The molecular structure of complex **L5**, with displacement ellipsoids drawn at the 50% probability level

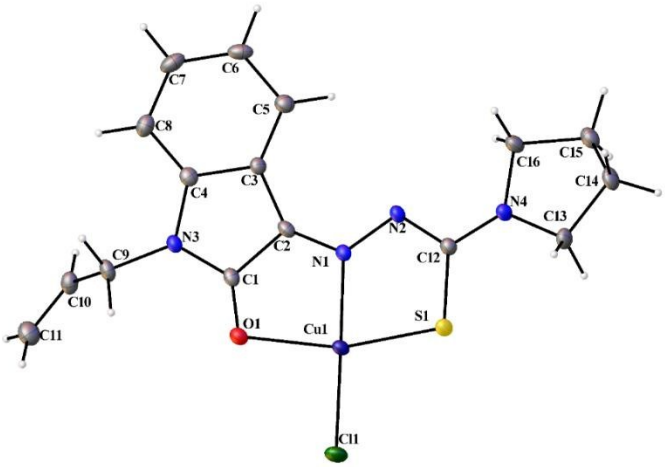

Fig. 8 The molecular structure of complex **3**, with displacement ellipsoids drawn at the 50% probability level

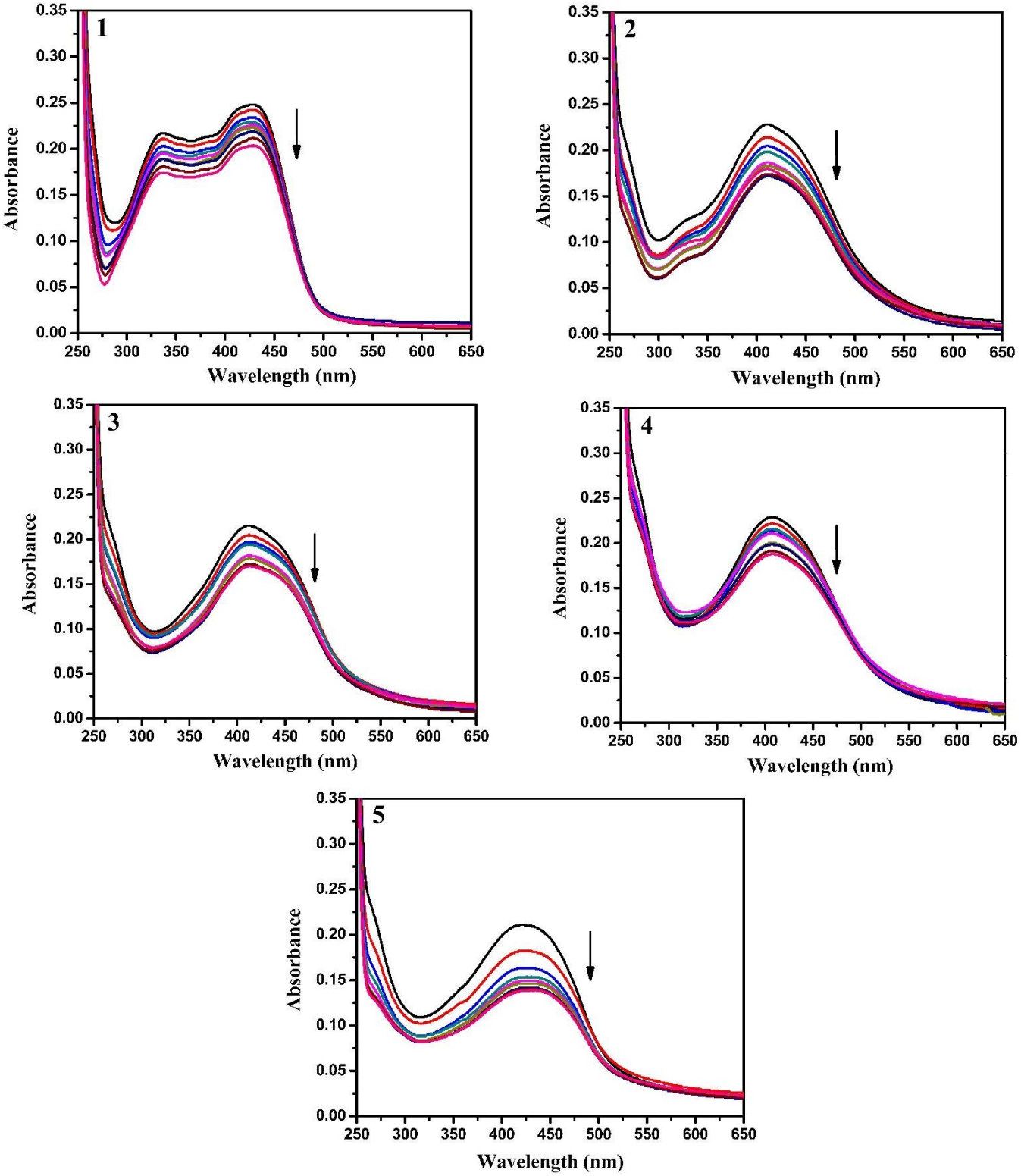

Fig. 9 Absorption spectra of complexes (**1**-**5**) in Tris-HCl buffer upon addition of CT DNA. [Complex] = 1.5 × 10^{-5} M, [DNA] = 0-40 µM. Arrow shows that the absorption intensities decrease upon increasing DNA concentration.

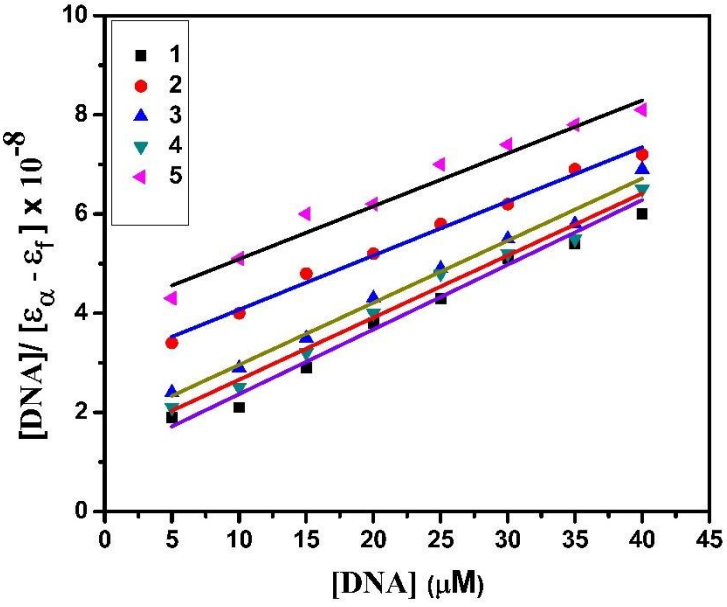

Fig. 10 Plots of [DNA]/($\varepsilon_a - \varepsilon_f$) *versus* [DNA] for the titration of the complexes with CT DNA.

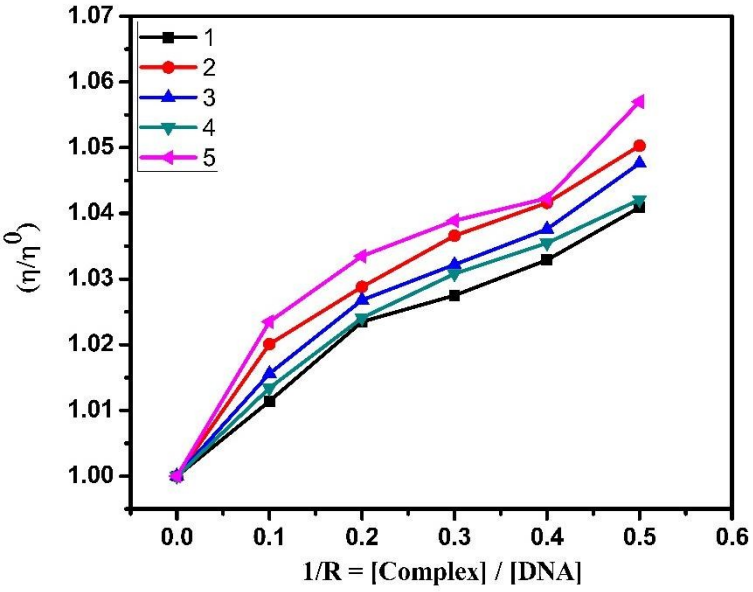

Fig. 11 Effect of the complexes on the viscosity of CT DNA (0.5 M).

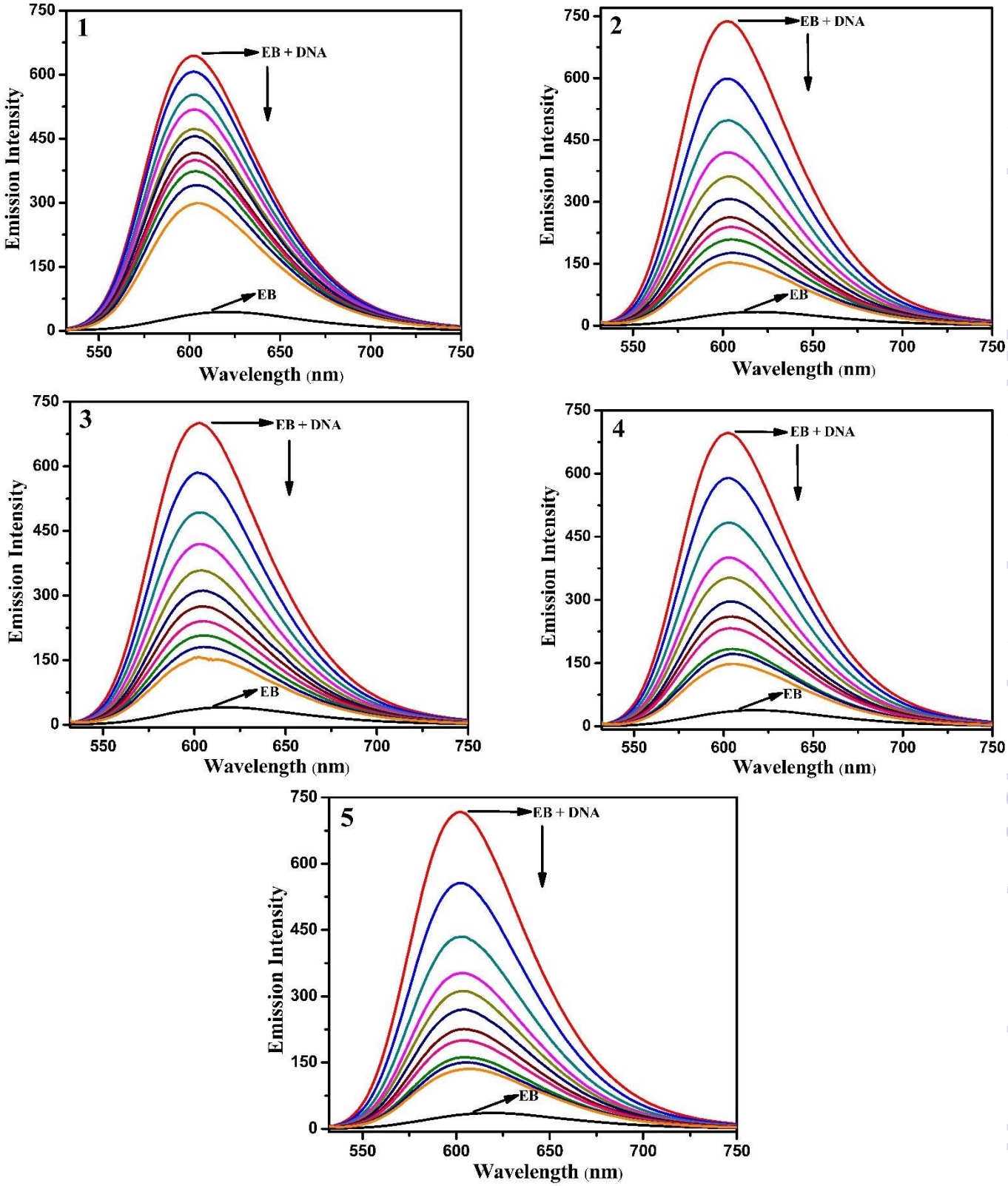

Fig. 12 Fluorescence quenching curves of EB bound to DNA in the presence of **1**-**5**. [DNA] = 5 µM, [EB] = 5 µM and [complex] = 0-50 µM.

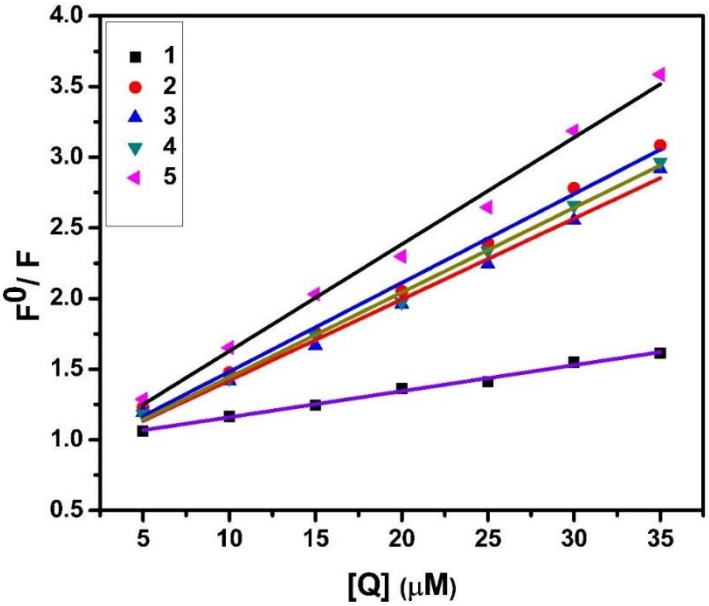

Fig. 13 Stern-Volmer plots of fluorescence titrations of the complexes with CT DNA.

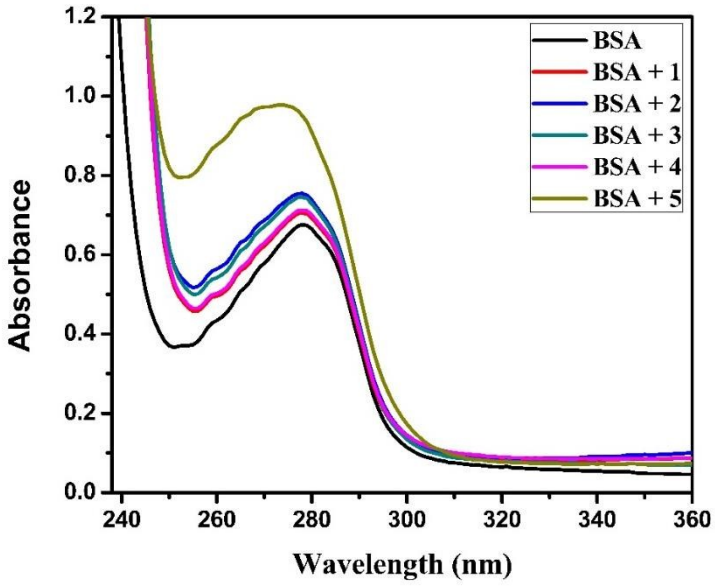

Fig. 14 The absorption spectra of BSA (10 μM) and BSA with **1**-**5** (4 μM).

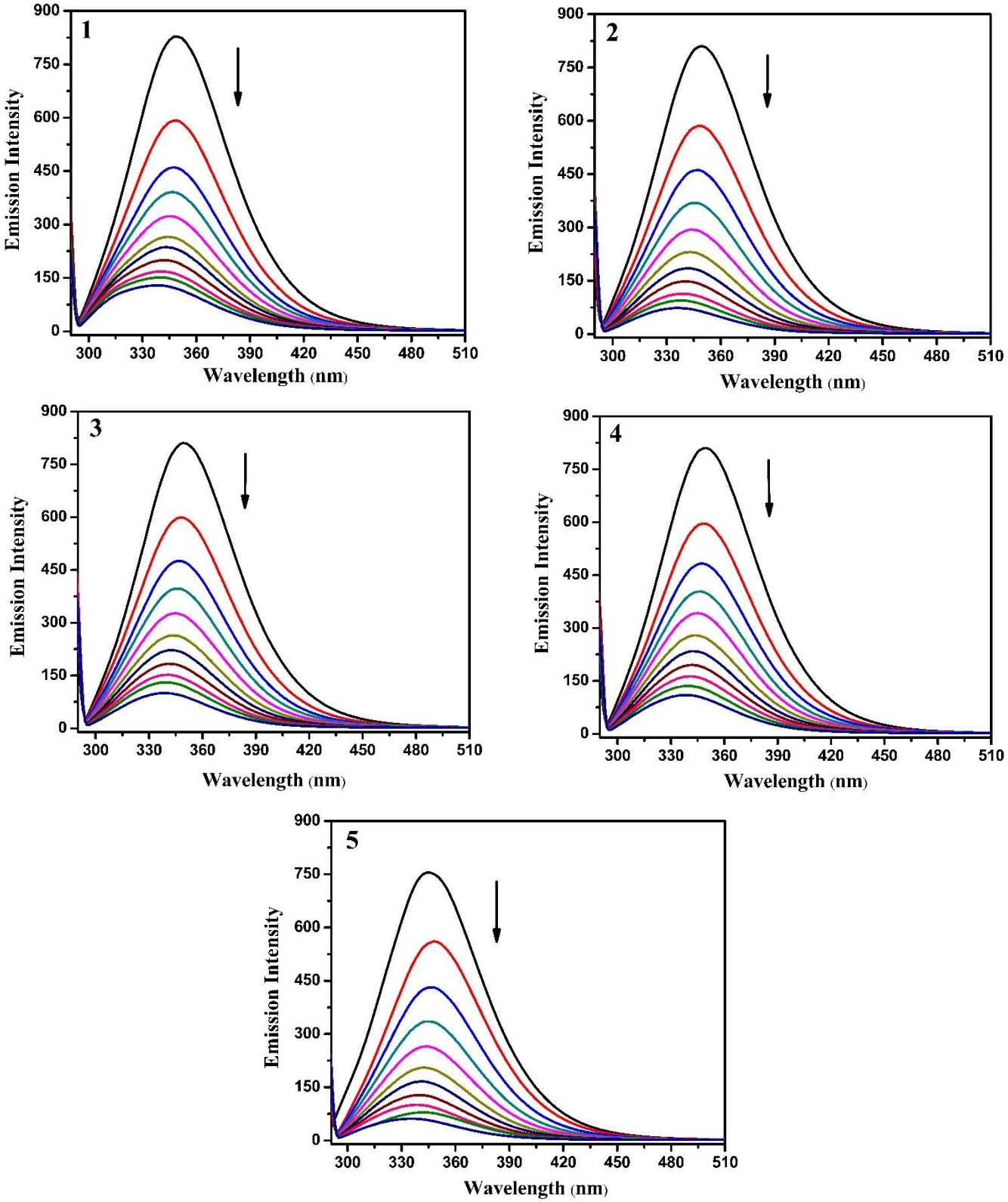

Fig.15 Fluorescence quenching curves of BSA in the absence and presence of **1-5**. [BSA] = 1 μM and [complex] = 0-20 μM.

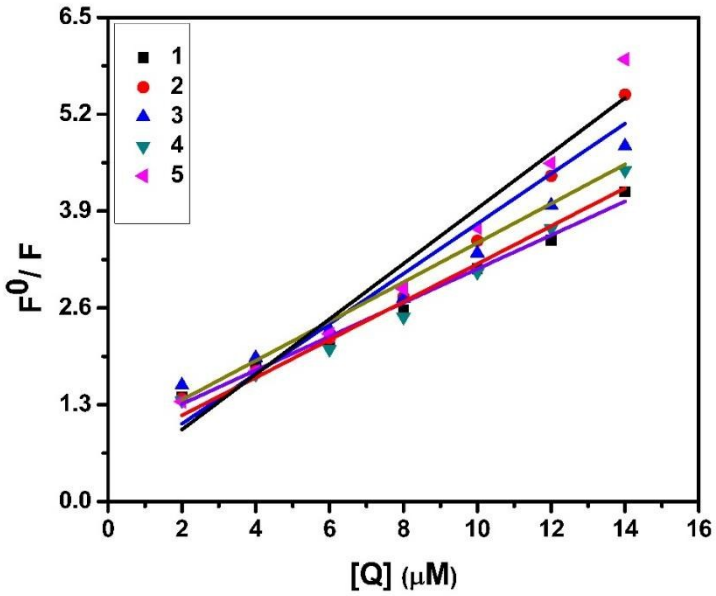

Fig. 16 Stern-Volmer plots of the fluorescence titrations of the complexes with BSA.

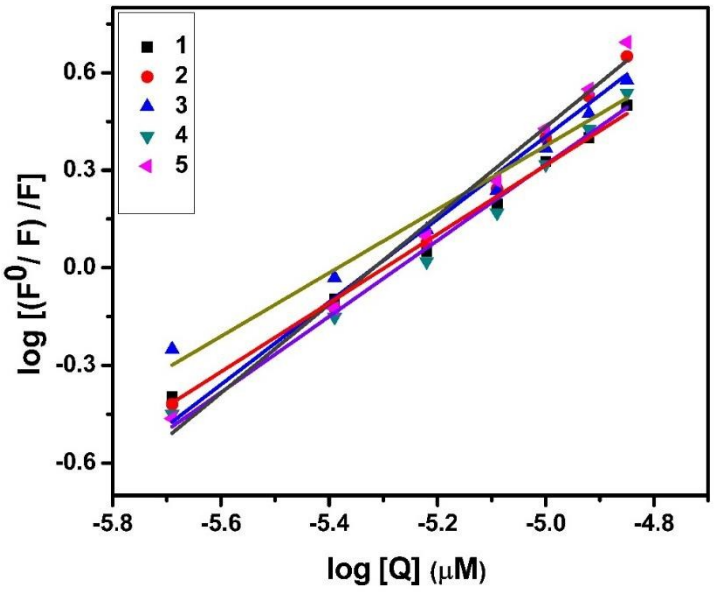

Fig. 17 Scatchard plots of the fluorescence titrations of the complexes with BSA.

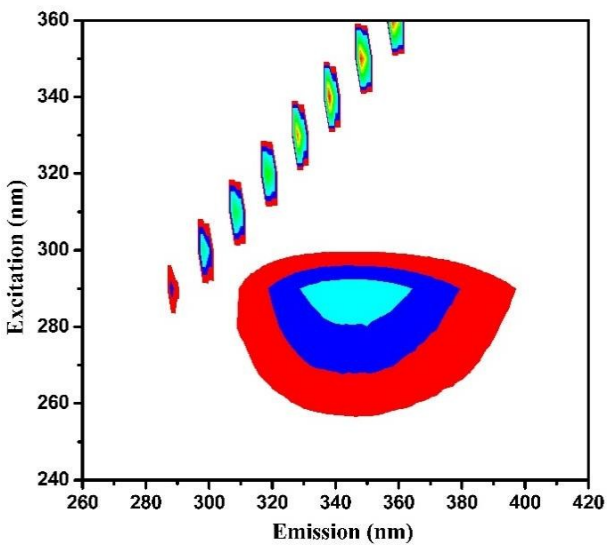

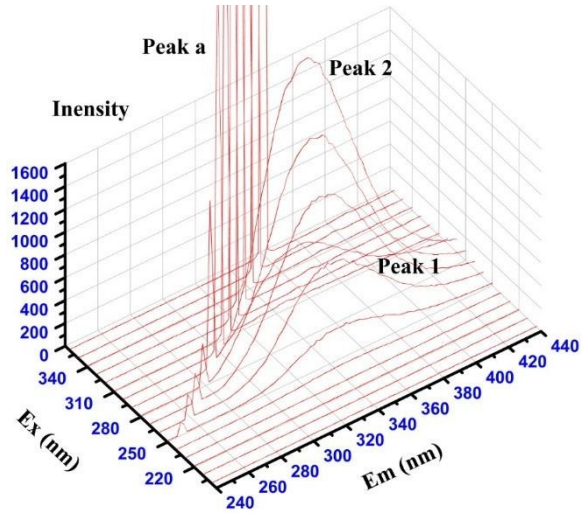

a

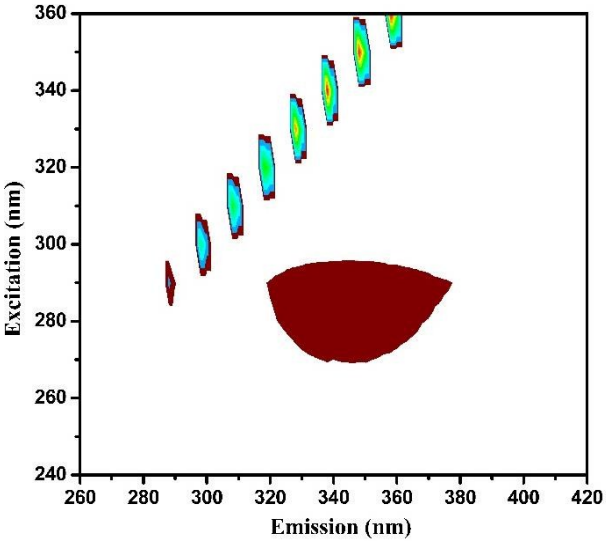

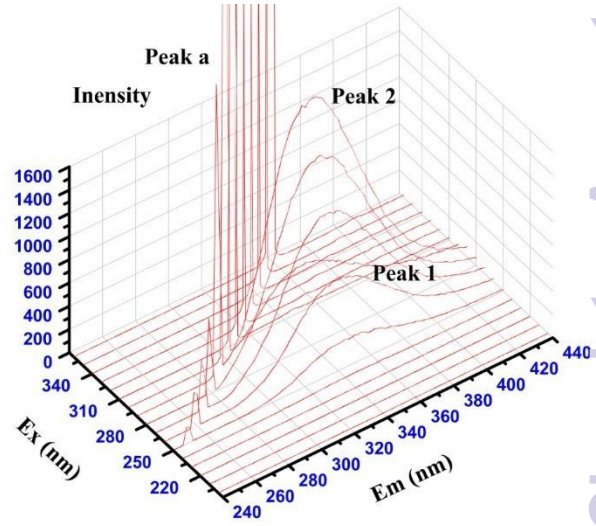

b

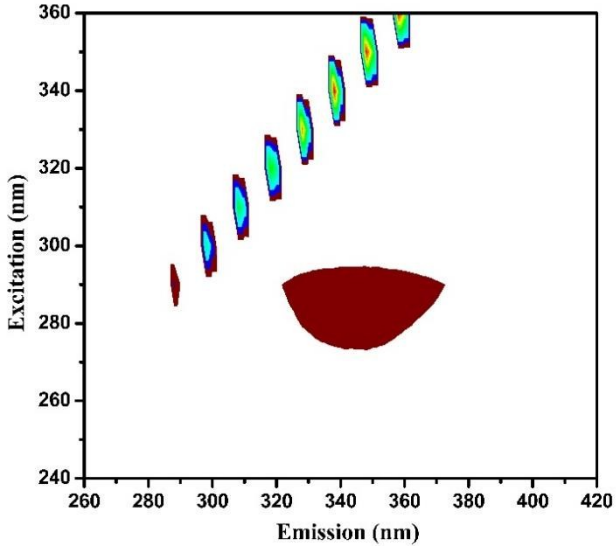

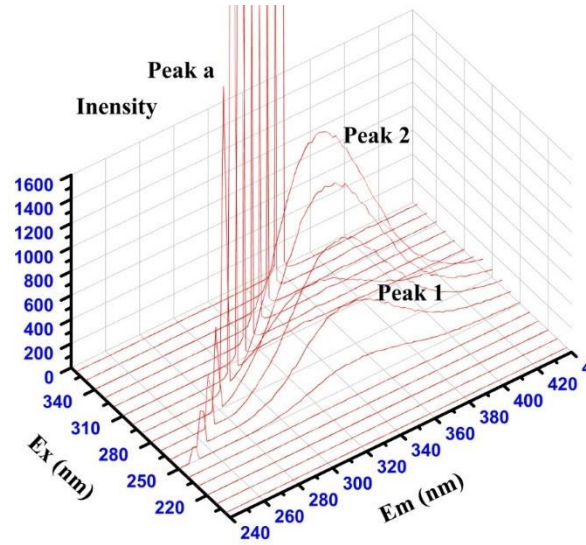

c

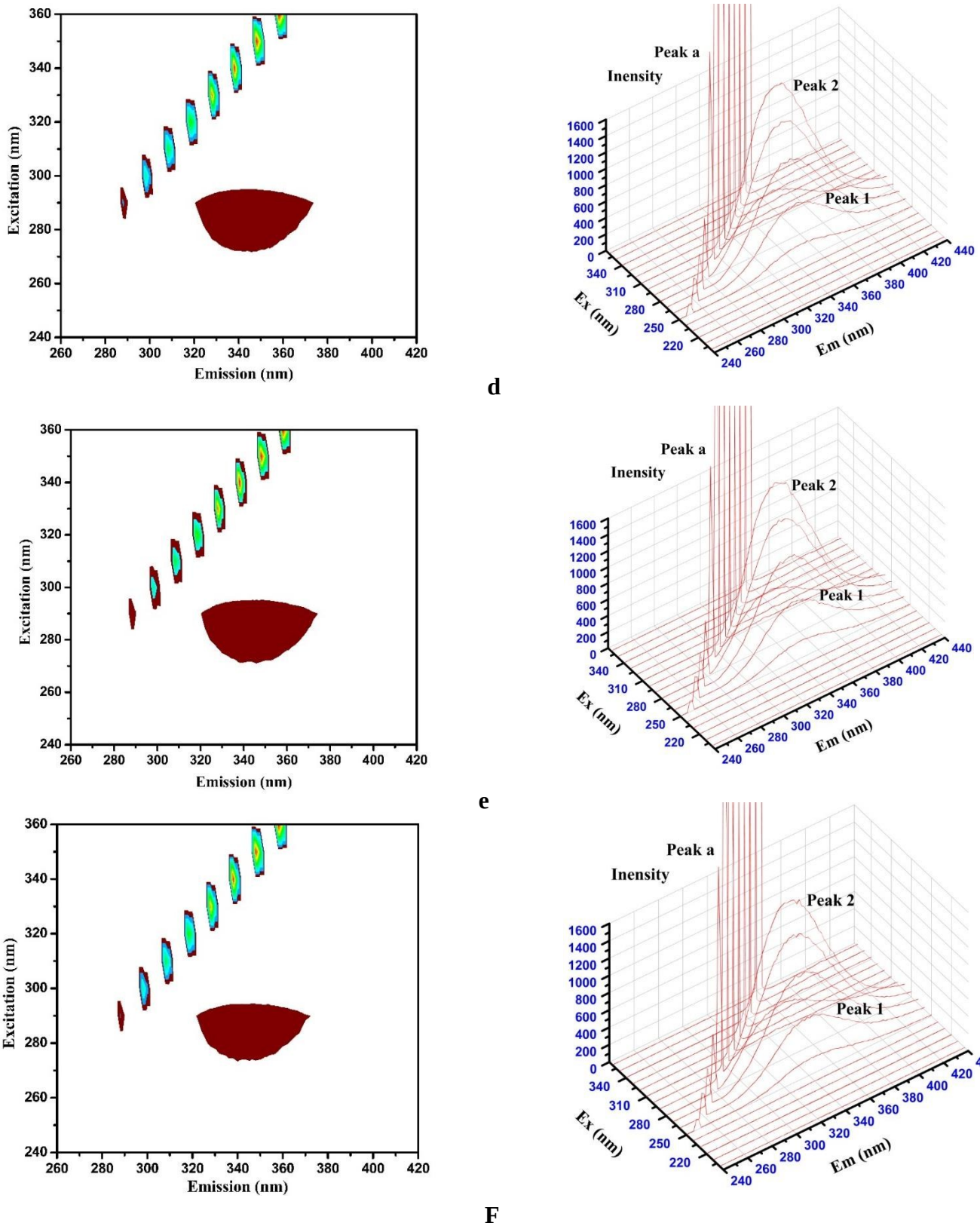

Fig.18 3D fluorescence spectra for (a) BSA (b) BSA-1 (c) BSA-2 (d) BSA-3 (e) BSA-4 and (f) BSA-5.

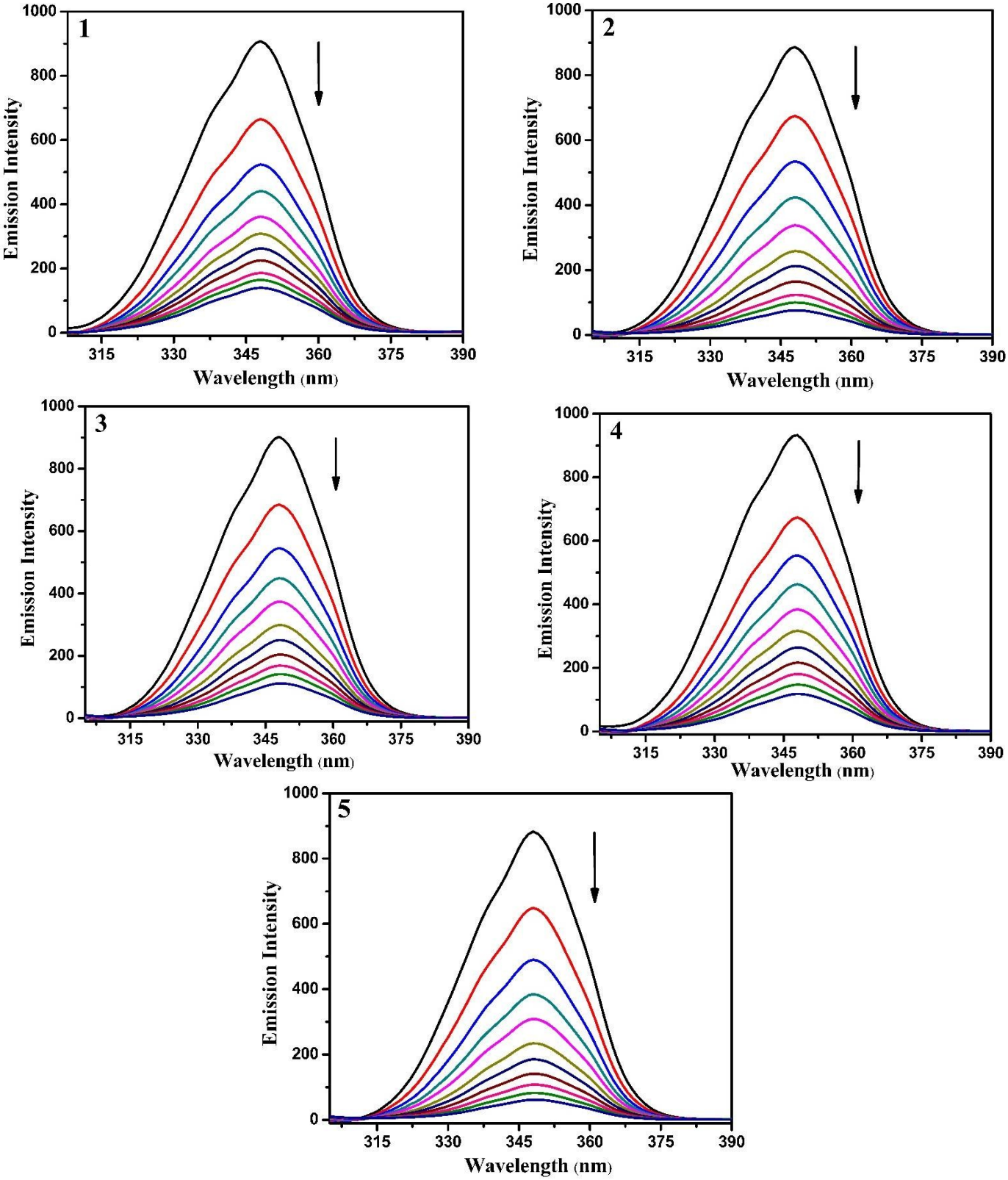

Fig. 19 Synchronous spectra of BSA (1 μM) as a function of concentration of **1-5** (0-20 μM) with $\Delta\lambda$ = 60 nm.

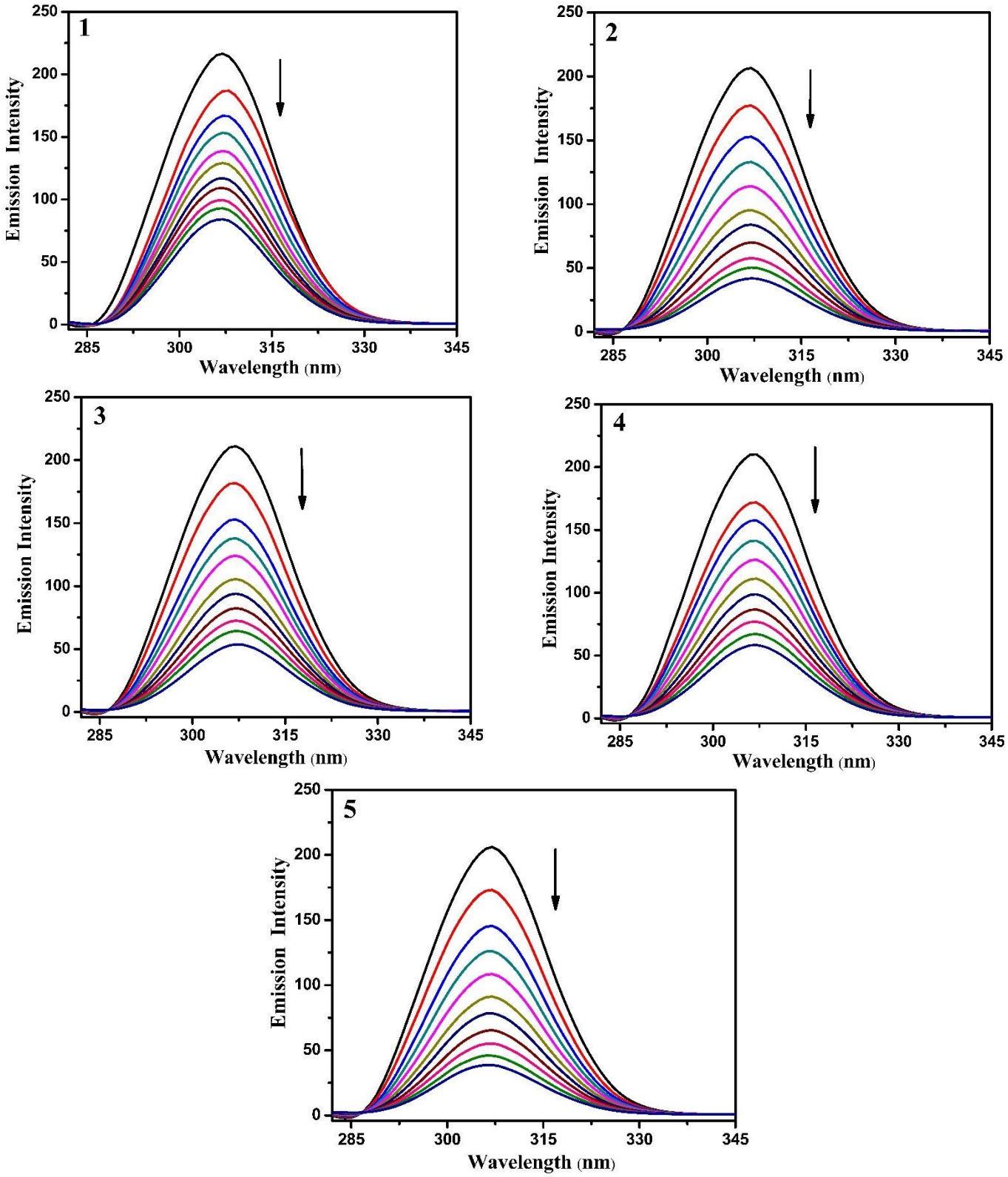

Fig. 20 Synchronous spectra of BSA (1 μM) as a function of concentration of **1-5** (0-20 μM) with $\Delta\lambda$ = 15 nm.

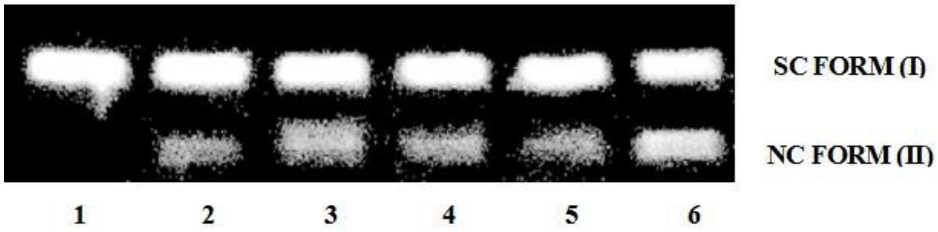

Fig. 21 Cleavage of supercoiled pUC19 DNA (30 μM) by complexes 1–5 in a buffer containing 5% DMF/5 mM Tris–HCl/50 mM NaCl at pH = 7.2 and 37 ^{o}C with an incubation time of 3 h. lane 1, DNA control; lane 2, DNA + 1 (150 μM); lane 3, DNA + 2 (150 μM); lane 4, DNA + 3 (150 μM); lane 5, DNA + 4 (150 μM); lane 6, DNA + 5 (150 μM). Forms SC and NC are supercoiled and nicked circular DNA, respectively.

Table 1 EPR parameters of Cu(II) complexes

Complex	Medium & Temp.	$g_{\parallel}$	$g_{\perp}$	$A_{\parallel}$ (MHz)
1	Solution state LNT	2.23	2.04	499
2	Solution state LNT	2.24	2.04	532
3	Solution state LNT	2.21	2.03	494
4	Solution state LNT	2.22	2.04	528
5	Solution state LNT	2.24	2.05	533

Table 2 Crystal data and structure refinement for ligands (L1-L5)

	L1	L2	L3	L4	L5
Empirical formula	$C_{13}H_{16}N_4O_2S$	$C_{16}H_{16}N_4OS$	$C_{16}H_{18}N_4OS$	$C_{18}H_{24}N_4OS$	$C_{20}H_{20}N_4OS$
Formula weight	292.36	312.39	314.40	344.47	364.46
Temperature (K)	110.15	110.15	110.15	150.15	110.15
Wavelength (Å)	0.71073	0.71073	0.71073	0.71073	0.71073
Crystal system	Monoclinic	Monoclinic	Monoclinic	Triclinic	Monoclinic
Space group	*P 1 21/c 1*	*C 1 2/c 1*	*C 1 2/c 1*	*P-1*	*P 1 21/n 1*
Unit cell dimensions					
a (Å)	12.365(9)	21.496(8)	21.514(19)	8.352(6)	8.0090(17)
b (Å)	15.377(11)	9.118(3)	9.287(7)	8.874(6)	19.621(4)
c (Å)	7.396(5)	15.908(5)	15.869(12)	13.617(9)	11.510(3)
α (°)	90	90	90	79.406(7)	90
β (°)	104.715(8)	108.156(6)	107.718(14)	81.424(7)	94.636(2)
γ (°)	90	90	90	64.639(7)	90
Volume ($Å^3$)	1360.2(16)	2962.7(18)	3020(4)	893.5(10)	1802.8(7)
Z	4	8	8	2	4
Density (Mg/m^3)	1.428	1.401	1.383	1.280	1.343
Absorption coefficient (mm^{-1})	0.246	0.226	0.222	0.194	0.196
F(000)	616	1312	1328	368	768
Crystal size (mm^3)	0.42 x 0.25 x 0.06	0.57 x 0.42 x 0.32	0.56 x 0.42 x 0.27	0.55 x 0.36 x 0.12	0.56 x 0.25 x 0.22
Theta range for data collection (°)	2.157 to 27.528	2.446 to 27.600	1.987 to 27.777	1.526 to 27.617	2.056 to 27.553
Index ranges	0<=h<=15, -19<=k<=19, -9<=l<=9	-27<=h<=27, -11<=k<=11, -20<=l<=20	-28<=h<=28, -12<=k<=12, -20<=l<=20	-10<=h<=10, -11<=k<=11, -17<=l<=17	-10<=h<=10, -23<=k<=25, -14<=l<=14

Reflections collected	5952	16644	16848	10379	15627
Independent reflections [R(int)]	3083 (0.0250)	3412 (0.0411)	3505 (0.0577)	4057 (0.0609)	4123 (0.0407)
Completeness to theta = 27.50°	99.5 %	99.8 %	99.8 %	99.8 %	99.8 %
Absorption correction	Semi-empirical from equivalents	Semi-empirical from equivalents	Semi-empirical from equivalents	Semi-empirical from equivalents	Semi-empirical from equivalents
Max. and min. transmission	0.746 and 0.664	0.7456 and 0.6943	0.7456 and 0.6561	0.7456 and 0.4874	0.7456 and 0.6501
Refinement method	Full-matrix least-squares on F^2	Full-matrix least-squares on F^2	Full-matrix least-squares on F^2	Full-matrix least-squares on F^2	Full-matrix least-squares on F^2
Data / restraints / parameters	3083 / 0 / 184	3412 / 0 / 199	3505 / 0 / 200	4057 / 0 / 218	4123 / 0 / 235
Goodness-of-fit on F^2	1.034	1.023	1.031	1.062	1.023
Final R indices [I>2sigma(*I*)]	R1 = 0.0384, wR2 = 0.0930	R1 = 0.0304, wR2 = 0.0749	R1 = 0.0385, wR2 = 0.0847	R1 = 0.0501, wR2 = 0.1176	R1 = 0.0404, wR2 = 0.0886
R indices (all data)	R1 = 0.0469, wR2 = 0.0974	R1 = 0.0345, wR2 = 0.0777	R1 = 0.0531, wR2 = 0.0920	R1 = 0.0731, wR2 = 0.1284	R1 = 0.0553, wR2 = 0.0962
Largest diff. peak and hole (e.$Å^{-3}$)	0.394 and -0.333	0.342 and -0.241	0.286 and -0.236	0.352 and -0.330	0.212 and -0.255

Table 3 Crystal data and structure refinement for complex **3**

	3
Empirical formula	$C_{16}H_{17}ClCuN_4OS$
Formula weight	412.38
Temperature (K)	150.15
Wavelength (Å)	0.71073
Crystal system	Triclinic
Space group	*P-1*
Unit cell dimensions	
a (Å)	a = 8.984(3)
b (Å)	b = 9.757(4)
c (Å)	c = 10.524(4)
α (°)	105.822(4)
β (°)	98.341(4)
γ (°)	108.844(4)
Volume ($Å^3$)	812.0(5)
Z	2
Density Mg/m^3	1.687
Absorption coefficient (mm^{-1})	1.649
F(000)	422
Crystal size (mm^3)	0.51 x 0.19 x 0.09
Theta range for data collection (°)	2.081 to 27.548
Index ranges	-11<=h<=11, -12<=k<=12, -13<=l<=13
Reflections collected	9526
Independent reflections [R(int)]	3682 (0.0410)
Completeness to theta = 27.50°	99.7 %
Absorption correction	Semi-empirical from equivalents

Max. and min. transmission	0.7456 and 0.5073
Refinement method	Full-matrix least-squares on F^2
Data / restraints / parameters	3682 / 0 / 217
Goodness-of-fit on F^2	1.063
Final R indices [I>2sigma(*I*)]	R1 = 0.0333, wR2 = 0.0879
R indices (all data)	R1 = 0.0382, wR2 = 0.0913
Largest diff. peak and hole (e.Å^{-3})	0.574 and -0.687

Table 4 Selected bond lengths (Å), angles (°) of ligands

	L1	**L2**	**L3**	**L4**	**L5**
S(1)-C(9)/C(12)/C(12)/C(14)/ C(16)	1.6718(19)	1.6823(13)	1.6708(18)	1.678(2)	1.6804(16)
O(1)-C(8)	1.234(2)	1.2333(15)	1.236(2)	1.237(2)	1.2294(18)
N(1)-C(1)	1.399(2)	1.4110(16)	1.411(2)	1.416(2)	1.411(2)
N(1)-C(8)	1.343(2)	1.3636(15)	1.356(2)	1.365(2)	1.3720(19)
N(2)-N(3)	1.3479(18)	1.3515(14)	1.350(2)	1.349(2)	1.3491(18)
N(2)-C(7)	1.291(2)	1.2952(16)	1.294(2)	1.304(2)	1.2928(19)
N(3)-H(3)	0.8800	0.8800	0.8800	0.8800	0.8800
N(3)-C(9)/C(12)/C(12)/C(14)/C(16)	1.369(2)	1.3784(15)	1.375(2)	1.388(2)	1.3791(19)
N(4)-C(9)/C(12)/C(12)/C(14)/C(16)	1.331(2)	1.3324(16)	1.332(2)	1.345(2)	1.334(2)
N(4)-C(10)/C(13)/C(13)/C(15)/C(17)	1.463(2)	1.4717(15)	1.466(2)	1.472(2)	1.4716(18)
N(4)-C(13)/C(16)/C(16)/C(18)/C(20)	1.470(2)	1.4807(15)	1.475(2)	1.490(2)	1.477(2)
C(1)-C(2)	1.374(2)	1.3842(17)	1.380(2)	1.379(3)	1.384(2)
C(1)-C(6)	1.400(2)	1.4033(16)	1.402(2)	1.412(2)	1.403(2)
N(1)-C(1)/C(8)/C(8)/C(8)/C(8)-C(6)/C(7)/C(7)/C(7)/C(7)	110.17(14)	106.36(10)	106.89(14)	106.63(16)	106.40(13)
N(2)-N(3)-C(9)/C(12)/C(12)/C(14)/C(16)	121.68(13)	121.45(10)	121.88(13)	120.85(15)	120.71(13)
N(2)-N(3)-H(3)	119.2	119.3	119.1	119.6	119.6

N(3)-C(9)/C(12)/C(12)/C(14)/C(16) -S(1)	123.80(12)	123.19(9)	123.42(13)	123.70(14)	122.87(12)
N(4)-C(9)/C(12)/C(12)/C(14)/C(16)-S(1)	123.52(13)	123.76(9)	123.89(12)	123.64(14)	123.50(12)
N(4)-C(9)/C(12)/C(12)/C(14)/C(16)-N(3)	112.68(14)	113.05(10)	112.69(13)	112.66(15)	113.63(14)
O(1)-C(8)-N(1)	127.02(15)	126.26(11)	125.90(15)	126.47(17)	126.40(15)
O(1)-C(8)-C(7)	126.06(15)	127.38(11)	127.21(15)	126.90(17)	127.49(14)

Table 5 Selected bond lengths (Å), angles (°) of complex **3**

	3
Cu(1)-S(1)	2.2463(7)
Cu(1)-O(1)	2.1079(15)
Cu(1)-N(1)	1.9743(18)
Cu(1)-Cl(1)	2.1791(9)
Cl(1)-Cu(1)-S(1)	99.05(3)
O(1)-Cu(1)-Cl(1)	95.89(5)
N(1)-Cu(1)-Cl(1)	175.13(15)
O(1)-Cu(1)-S(1)	161.66(15)
N(1)-Cu(1)-S(1)	83.51(6)
N(1)-Cu(1)-O(1)	82.42(7)
N(2)-N(1)-Cu(1)	125.16(13)
C(1)-O(1)-Cu(1)	105.87(13)
C(2)-N(1)- Cu(1)	113.91(13)
C(12)-S(1)- Cu(1)	95.78(3)

Table 6 DNA binding constant (K_b), Stern-Volmer constant (K_q) and the apparent binding constant (K_{app}) for complexes **1-5**

Complex	K_b (M^{-1})	K_q (M^{-1})	K_{app} (M^{-1})
1	$1.06 \times 10^4 \pm 0.12$	$1.84 \times 10^4 \pm 0.15$	$9.21 \times 10^5 \pm 0.01$
2	$1.39 \times 10^4 \pm 0.14$	$6.28 \times 10^4 \pm 0.04$	$3.14 \times 10^6 \pm 0.01$
3	$1.23 \times 10^4 \pm 0.13$	$5.99 \times 10^4 \pm 0.04$	$2.99 \times 10^6 \pm 0.02$
4	$1.20 \times 10^4 \pm 0.17$	$5.72 \times 10^4 \pm 0.03$	$2.86 \times 10^6 \pm 0.01$
5	$2.09 \times 10^4 \pm 0.09$	$7.55 \times 10^4 \pm 0.06$	$3.77 \times 10^6 \pm 0.01$

Table 7 Protein binding constant (K_b), quenching constant (K_q) and number of binding sites (n) for complexes **1-5**

Complex	K_b (M^{-1})	K_q (M^{-1})	n
1	$4.06 \times 10^5 \pm 0.08$	$2.26 \times 10^5 \pm 0.16$	1.05
2	$5.78 \times 10^6 \pm 0.15$	$3.35 \times 10^5 \pm 0.33$	1.27
3	$1.43 \times 10^6 \pm 0.30$	$2.63 \times 10^5 \pm 0.1$	1.16
4	$1.08 \times 10^6 \pm 0.15$	$2.54 \times 10^5 \pm 0.27$	1.12
5	$1.77 \times 10^7 \pm 0.24$	$3.71 \times 10^5 \pm 0.31$	1.36

Table 8 Self-activated cleavage data of SC pUC19 DNA (30 μM) by complexes **1-5** (150 μM) for an incubation time of 3 h

Lane No	DNA control	Percentage of cleavage (C) (%)	
		SC	NC
1	DNA	100	0
2	DNA + **1** (150 μM)	88.1	11.8
3	DNA + **2** (150 μM)	74.9	25.0
4	DNA + **3** (150 μM)	79.0	20.9
5	DNA + **4** (150 μM)	81.9	18.0
6	DNA + **5** (150 μM)	51.9	48.0

Table 9 3D fluorescence spectral characteristics of BSA and BSA with complexes (**1–5**)

System	Peak 2 λ_{ex} /λ_{em}	$\Delta\lambda$	Intensity
BSA	280/343	60	1511
BSA-**1**	280/339	59	1196
BSA-**2**	280/335	55	990
BSA-**3**	280/336	56	1002
BSA-**4**	280/337	57	1019
BSA-**5**	280/332	52	823

Synthesis, X-ray crystal structure, DNA/protein binding and DNA Cleavage Studies of Novel Copper(II) Complexes of N-substituted isatin thiosemicarbazone ligands

Graphical abstract